



**Politecnico
di Torino**

Master's Degree in Environmental and Land Engineering
Climate Change

**Automatic Mapping of irrigation grid of Cavour Channel
through aerial multispectral data**

Candidate

Donya Deris Zadeh s301232

supervisors

Prof. Francesca Matrone

Prof. Stefania Tamea

Prof. Andrea Maria Lingua

2024

Table of Contents

| | |
|---|----|
| Abstract..... | g |
| Acknowledgement | h |
| 1. Introduction..... | 1 |
| 1.1. Overview of the Cavour Channel..... | 2 |
| 1.1.1. Infrastructure..... | 2 |
| 1.1.2. Seasonal operation management..... | 2 |
| 1.1.3. The role of the Farini channel | 3 |
| 1.2. Importance of studying irrigation networks..... | 4 |
| 1.3. The irrigation network of Piemonte | 5 |
| 1.4. Aims and expected results..... | 6 |
| 2. Study area and data | 7 |
| 2.1. Study area and data | 7 |
| 2.2. Role of the NIR and visible bands for water detection | 10 |
| 2.3. Importance of resolution of the images..... | 11 |
| 2.4. Importance of resolution of DTM data | 12 |
| 3. Methods and results | 13 |
| 3.1. Methodology..... | 13 |
| 3.1.1. The choice of supervised classification with respect to the unsupervised approach..... | 15 |
| 3.1.2. Supervised pixel-based classification for water detection | 16 |
| 3.2. Workflow | 17 |
| 3.2.1. First level classification: CIR image..... | 17 |
| 3.2.2. Second level classification: RGB Image..... | 28 |
| 3.2.3. Creation of buffers for channels..... | 34 |
| 3.2.4. Evaluation of performance of each classifier..... | 36 |
| 3.2.5. Validation of classification result | 42 |
| 3.2.6. Extraction of channel polygons..... | 52 |

| | |
|--|----|
| 3.2.7. Accuracy assessment..... | 58 |
| 3.2.8. Determining the flow direction in channels..... | 65 |
| 4. Discussion..... | 70 |
| 4.1. Improvement of channel documentation and flow direction detection..... | 70 |
| 4.2. Multi temporal analysis using channel geometry and Sentinel-2 data..... | 73 |
| 4.3. Classification challenges and spectral coverage limitations | 73 |
| 4.4. Necessity of repetition of the acquisition..... | 74 |
| 4.5. Classifier selection and performance | 74 |
| 4.6. An open challenge..... | 74 |
| 5. Conclusion | 76 |
| Bibliography | 78 |

List of figures

| | |
|---|----|
| Figure 1- The entrance culvert of the Cavour channel in Chivasso - West Sesia Irrigation Association..... | 1 |
| Figure 2- The CIR image composing of 3 bands of Green-Red-Near Infrared | 8 |
| Figure 3- The RGB image composing of 3 bands of Blue-Green-Red..... | 8 |
| Figure 4- The Digital Elevation Model with 5 meters pixel size and 1 meter resolution in elevation, the values of elevation are reported in meter, from 0 to 204 m | 9 |
| Figure 5- The line features of the channels, with 3 levels, where level 0 represents natural streams and rivers, level 1 represents the main channels like Cavour, and level 2 represents the principal irrigation channels | 9 |
| Figure 6- Signature of clear water versus turbid water , focusing on difference of reflectance of clear and turbid water..... | 11 |
| Figure 7- Graphical workflow of methodology | 13 |
| Figure 8- The CIR image, input data of the first level classification | 17 |
| Figure 9- Generating the shape file of the training samples using the tool of "Training sample Manager"..... | 18 |
| Figure 10- The K-nearest neighbor classifier..... | 19 |
| Figure 11- The random trees classifier..... | 20 |
| Figure 12- The support vector machine classifier..... | 21 |
| Figure 13- The maximum likelihood Classifier..... | 22 |
| Figure 14- The classified raster of K nearest neighbor | 23 |
| Figure 15- The classified raster of SVM..... | 23 |
| Figure 16- The classified raster of random trees..... | 24 |
| Figure 17- The classified raster of maximum likelihood | 24 |
| Figure 18- Water pixels resulting from the random trees classifier | 25 |
| Figure 19- Water pixels resulting from the support vector machine classifier..... | 25 |
| Figure 20- Water pixels resulting from the K nearest neighbor classifier..... | 26 |
| Figure 21- Water pixels resulting from the maximum likelihood classifier..... | 26 |
| Figure 22- Water polygons aggregated from all of the four classifiers performed in the first level of classification | 27 |
| Figure 23- The RGB image masked by the aggregated water polygons of figure 21, which is input of the second level classification..... | 28 |
| Figure 24- Training samples of the second level classification | 28 |
| Figure 25- The second level classified raster of the K-nearest neighbor classifier..... | 29 |

| | |
|--|----|
| Figure 26- The second level classified raster of the SVM classifier..... | 30 |
| Figure 27- The second level classified raster of the random trees classifier..... | 30 |
| Figure 28- The second level classified raster of the maximum likelihood classifier | 31 |
| Figure 29- Water pixels resulting from the random forest classifier of the second level..... | 31 |
| Figure 30- Water pixels resulting from the maximum likelihood classifier of the second level..... | 32 |
| Figure 31- Water pixels resulting from the SVM classifier of the second level | 32 |
| Figure 32- Water pixels resulting from the K-nn classifier of the second level..... | 33 |
| Figure 33- Water polygons aggregated from all of the four classifiers performed in the second level of classification, which is considered as the final result of water pixels from the classification step..... | 33 |
| Figure 34- The buffers of the channels | 34 |
| Figure 35- The buffer of one segment channel holds all the water polygons related to that segment of the channel | 35 |
| Figure 36- The binary raster of water and non-water of K nearest neighbor classifier..... | 36 |
| Figure 37- The binary raster of water and non-water of SVM classifier | 37 |
| Figure 38- The binary raster of water and non-water of random trees classifier | 37 |
| Figure 39- The binary raster of water and non-water of maximum likelihood classifier..... | 38 |
| Figure 40- The Weight raster of classifiers, which is the sum of the four binary rasters | 38 |
| Figure 41- The weight raster masked for the buffers of the channels..... | 39 |
| Figure 42- The training zone and the test zone for validation of the classification | 42 |
| Figure 43- Input data of scenario 1 is only the water pixels resulted from classification which belong to the water channels..... | 43 |
| Figure 44- Input data of scenario 2 is all of the pixels detected as water in the classification step | 44 |
| Figure 45- Scenario 1 : histogram of the water pixels versus the full subset , unit of pixel intensity : digital number | 45 |
| Figure 46- Scenario 2 : histogram of the water pixels versus the full subset , unit of pixel intensity : digital number | 45 |
| Figure 47- The model does not serve for detection of major water bodies such as lakes | 50 |
| Figure 48- Application of the model to the test zone | 51 |
| Figure 49- The scattered polygons detected as water channel | 52 |
| Figure 50- Polygons converted to points located at their centroid..... | 53 |
| Figure 51- Lines are generated from the points | 53 |
| Figure 52- Rectangles are generated along the lines..... | 54 |
| Figure 53- The rectangles are dissolved..... | 54 |
| Figure 54- The dissolved rectangles are smoothed..... | 55 |

| | |
|--|----|
| Figure 55- Model builder to generate polygons of channels from the scattered water polygons | 56 |
| Figure 56- Model Builder with iteration to propagate the generation of the channels polygons to the entire subset | 57 |
| Figure 57- Final result of the model , every piece of channel is generated | 58 |
| Figure 58- The accurate sample1 | 60 |
| Figure 59- Channel polygons generated by the model, sample1 | 60 |
| Figure 60- The omission error of sample 1 | 61 |
| Figure 61- The commission error of sample 1 | 61 |
| Figure 62- The accurate sample2 | 62 |
| Figure 63- Channel polygons generated by the model, sample 2 | 62 |
| Figure 64- The omission error of sample 2 | 63 |
| Figure 65- The commission error of sample 2 | 63 |
| Figure 66- The Digital Elevation Model with 5 meters pixel size and 1 meter resolution in elevation, the values of elevation are reported in meter, from 0 to 204 m | 65 |
| Figure 67- The line features of the channels, with 3 levels, where level 0 represents natural streams and rivers, level 1 represents the main channels like Cavour, and level 2 represents the principal irrigation channels | 66 |
| Figure 68- The end points of the channels | 67 |
| Figure 69- Direction of flow determined by arrows between 2 points | 68 |
| Figure 70- Model builder to generate arrowed line between 2 points which determines the direction of flow | 69 |
| Figure 71- The model could successfully detect the existing recorded channels and many unrecorded ones | 70 |
| Figure 72- Bar chart of time consumed for each step of the work | 72 |
| Figure 73- The CIR image | 75 |
| Figure 74- Imagery base map of ArcGIS pro | 75 |

List of tables

| | |
|--|----|
| Table 1- Number of detected water pixels related to each wight of 0 to 4..... | 40 |
| Table 2- True positive and false positive values for each coefficient of standard deviation in the scenario 1 | 46 |
| Table 3- True positive and false positive values for each coefficient of standard deviation in the scenario 2 | 47 |
| Table 4- Results of scenario 1, unit : digital number | 48 |
| Table 5- Results of the scenario 2 , unit : digital number | 48 |
| Table 6- Accuracy assessment of the model to generate polygons of the channels | 64 |
| Table 7- Time consumed on each step of the work..... | 71 |

Abstract

This study presents a comprehensive approach to the automatic mapping and analysis of the irrigation grid of the Cavour Channel, located in Piemonte, Italy, addressing the unique challenges of applying the methodology to larger irrigation systems.

The study focuses on identifying irrigation channels using aerial multispectral data to create a polygon feature of channels and determine flow directions in the channels. The research uses supervised pixel-based classification methods on CIR (Color-Infrared) and RGB orthophotos for the detection of water bodies, using four classification algorithms: K-Nearest Neighbor, Random Trees, Support Vector Machine, and Maximum Likelihood. The classification performance and effectiveness of each algorithm are assessed by comparing the result of each classifier, aiming to improve the water detection process for these narrow, complex irrigation channels.

Following the classification step, the results are simplified to some mathematical models, in order to pick the best one that simulates the results of classification. The models are trained based on histogram analysis of each band of data. The purpose of this step is to validate the process of classification in order to assess their capability of propagation for other study areas.

The detected water pixels were then used to generate polygons, representing the irrigation channels within the study area. Buffer zones around channel features are created to ensure that polygons accurately reflect channel segments while excluding misclassified pixels of shadows or roads. A model using the tools of ArcGIS pro is introduced to generate polygons of channels from their scattered pixels.

Ultimately Digital Terrain Model (DTM) together with line features of the channels are used to determine the flow directions in each channel segment. This step is performed based on elevation differences between the two endpoints of each channel, so that the flow across the irrigation network may be visualized.

Acknowledgement

I would like to express my sincere gratitude to Professors Francesca Matrone, Stefania Tamea, and Andrea Maria Lingua for their invaluable guidance, expertise, and support throughout the course of this research. Their insights and encouragement have been instrumental in the development of this study. I am also deeply thankful to Ovest Sesia Organization of Irrigation team particularly to Livio Bourbon for his generous hospitality and for providing access to essential resources that were crucial to this work.

I hope that the findings of this study contribute to a deeper understanding of the irrigation network conditions and serve to enhance the quality of management practices. Such improvements are vital for promoting a more sustainable future in agriculture and irrigation, helping to secure water resources and support resilient agricultural practices.

1. Introduction



Figure 1- The entrance culvert of the Cavour channel in Chivasso - West Sesia Irrigation Association

1.1. Overview of the Cavour Channel

The Cavour Channel, located in the northern Italy, Piemonte, is an 83-kilometer-long artificial waterway, stands as one of the most significant hydraulic engineering projects in Italy. Designed to irrigate vast agricultural lands, primarily rice fields. it plays a critical role in Northern Italy's agricultural economy, particularly in the Piedmont and Lombardy regions. The channel begins in Chivasso, in the province of Turin, and ends in Galliate, in the Novara province, where it discharges the Ticino River, a tributary of the Po River. From its inception, the Cavour Channel has been an essential water source, facilitating the efficient irrigation of approximately 500,000 hectares of agricultural land, primarily devoted to rice cultivation, was constructed between 1863 and 1866, under the direction of Italian statesman Camillo Benso, Count of Cavour. It was part of a broader vision to improve agricultural productivity in Italy's fertile Po Valley. The Po River, which runs through Northern Italy, is the primary water source for the Channel. At Chivasso, the Po's waters are diverted into the Cavour Channel via a reinforced inlet that is approximately 40 meters wide, completely paved with pebbles, concrete and stone slabs.

1.1.1. Infrastructure

The Cavour Channel features an impressive network of hydraulic structures that have remained largely intact since its construction. These include 210 siphons, 101 bridges, and 62 aqueducts, making the Channel a masterpiece of 19th-century engineering. These structures help the Channel traverse the region's varied terrain, enabling the smooth flow of water over long distances. Despite being more than 170 years old, many of these original constructions are still functional, a testament to the durability and ingenuity of the Channel's design.

The Channel is part of a broader irrigation system that spans 1,500 kilometers, connecting to other major Channels such as the Regina Elena Channel, which was added in 1954. This extensive network ensures that water is distributed efficiently across a wide region, supporting not only rice cultivation but also other types of agriculture[1][2].

1.1.2. Seasonal operation management

The Cavour Channel operates seasonally, with its active period running from early May to mid-September, aligning with the irrigation season. This operational window is crucial for the irrigation of rice fields, which require substantial water resources during the warmer months. Outside of this period, the Channel is completely emptied, and the entire network remains dry until the following spring. This seasonal cycle reflects the needs of Northern Italy's agricultural calendar, ensuring that water is available during peak growing periods while conserving resources in the off-season.

The water distribution process within the Channel system is managed in a stepped manner, a technique designed to maximize irrigation efficiency. Irrigation begins in the upstream sections of the Channel, where each area is flooded for two to three weeks before the water is allowed to flow downstream to the next section. This staged approach ensures that each area receives adequate water, and that water resources are conserved as they flow through the entire irrigation system. This system of managing movement of water is performed only based on gravity and without use of any external energy.

Once the irrigation process is complete, the remaining water in the system is returned to the Po River basin, particularly at the point where the Cavour Channel meets the Po and Sesia rivers. This cyclical use of water ensures that no excess water is wasted, and the water resources are sustainably managed within the broader Po Valley ecosystem[3].

1.1.3 The role of the Farini channel

The Cavour channel on the Po River as its primary water source has posed challenges, particularly during the hot summer months when water levels in the Po can drop significantly. To address this issue, the Farini Channel was constructed in 1868, just two years after the Cavour Channel was completed. The Farini Channel brings additional water into the Cavour Channel by diverting water from the Dora Baltea, a river with a more consistent water flow than the Po, particularly during the summer.

The Farini Channel connects with the Cavour Channel between cities of Saluggia and Crescentino, where it helps to regulate the water temperature and flow. The cold waters of the Dora Baltea mix with the warmer waters of the Po, ensuring that the Cavour Channel maintains an adequate water supply even during periods of exceptionally low flow in the Po River. This strategic blending of water sources allows the Cavour Channel to continue operating at full capacity during critical summer months[4].

1.2. Importance of studying irrigation networks

According to the United Nations' prospects, by 2030, the world's population is expected to grow to over 8.5 billion, leading to increased demand for food, water, and energy. To meet these needs, the United Nations estimates a need for 35% more food, 40% more water, to prevent critical shortages. Since only about 3% of Earth's water is available for human use, managing water for irrigation efficiently is essential. Improving irrigation practices will help meet the growing food demand and make the best use of limited water resources [5]. The agricultural sector stands out as the primary user of freshwater resources, accounting for the majority of both water withdrawal and overall water consumption. Specifically, agriculture is responsible for approximately 70% of total water withdrawals globally and a striking 90% of consumptive water use—water that is not returned to its source after use. In comparison, municipal uses such as residential and public services require about 10% water withdrawals, while industrial activities account for around 20% [6]. Rice production is highly water-intensive, with approximately 3,400 liters of water needed to produce just one kilogram of rice. To put this into perspective, this amount of water is equivalent to the daily water needs of 34 individuals, assuming an average personal consumption of 100 liters per day. This substantial water footprint highlights the significant resources required to grow staple crops like rice, underscoring the environmental implications of water use in agriculture [7].

As populations grow, future projections indicate a significant rise in water demand. This anticipated increase in water consumption is driven not only by the sheer rise in the number of people but also by the changing lifestyle expectations that accompany economic growth and development. These trends place additional pressures on existing water resources, intensifying the challenge of sustainable water management to meet both agricultural and domestic needs [8].

Advances in understanding irrigation systems and the internal processes that govern them have significantly enhanced our ability to assess how changing conditions impact these systems and, in turn, how the systems affect the surrounding environment. With a deeper understanding of these dynamics, we can obtain detailed insights that serve as a strong foundation for decision-makers to design and implement effective, informed strategies. This knowledge is crucial for advancing climate-smart agriculture, helping to ensure that agricultural practices are resilient to climate change, resource-efficient, and sustainable in the long term [9] [10].

1.3. The irrigation network of Piemonte

Italy is the leading rice producer in Europe, with an annual production of 1.4 million tons cultivated across 220,000 hectares. Rice farming in Italy relies on submerged irrigation, which often has low efficiency and can lead to water-related conflicts [11].

Additionally, the Mediterranean region is recognized as a climate change hotspot, with projected increases in temperature, reduced precipitation, and more frequent and severe extreme events such as floods and droughts [12]. The seasonal distribution of rainfall is also expected to shift [13]. Mountains in the Mediterranean serve as essential sources of water for the lower-lying basins, supplying water for irrigation and other needs. Recent studies indicate that by the mid-21st century, almost 1.5 billion people will depend on mountain runoff [14]. These mountainous regions, however, are particularly sensitive to climate variability

In semi-arid basins, plains experience low rainfall, high evapotranspiration, and deep unsaturated zones, while piedmont areas, located between mountains and plains, benefit from milder climates and water runoff, making them ideal for agriculture [15]. Traditional irrigation systems in these regions use gravity-fed channels to divert floodwater for irrigation, supporting both agriculture and groundwater recharge [16].

In Piemonte region The Cavour channel, along with other channels located on upper streams such as Depretis and Farini channel, has historically provided reliable irrigation to agricultural fields in the Piemonte region by utilizing water from the Po and Dora Baltea rivers [2].

However, Recent studies emphasize the urgent need to reconsider irrigation practices in the Mediterranean region due to anticipated climate changes. Rising temperatures, reduced precipitation, and more frequent and severe drought events are expected to decrease water availability, making efficient irrigation crucial to sustain agricultural productivity and reduce water stress. Recent research highlights that updating irrigation systems with climate-adaptive practices, such as precision irrigation, can help mitigate these impacts and improve water efficiency in Mediterranean agriculture. As water scarcity intensifies, these adaptive strategies are essential for sustainable agricultural management in this vulnerable region [17].

1.4. Aims and expected results

The primary objective of this study is to discover location of the channels based on high resolution multispectral aerial data, and to create a detailed map of the irrigation network as a polygon feature. This map will serve as a reference for multi-temporal analysis, allowing for the evaluation of changes in the presence and quantity of water within the channels over time. In addition, it is aimed at determining the flow direction of each channel section based on data from a digital terrain model (DTM), providing further insights into water distribution within the network.

2. Study area and data

2.1. Study area and data

The study area is a rectangular region located northeast of Torino, within the Piedmont region. The approximate coordinates for two opposite vertices of this rectangle are [8.000° E, 45.240° N] and [8.136° E, 45.198° N], covering a total area of approximately 51 square kilometers.

The Cartographic Sector of Regione Piemonte has provided several valuable topographic products for local-level planning, which are available in the Geomatic Lab of the Politecnico di Torino. This research has made use of RGB and CIR (color-infrared) orthophotos, both with a geometric resolution of 0.4 meters. The RGB orthophotos consist of three spectral bands: blue, green, and red. The CIR orthophotos are composed of green, red, and near-infrared bands. Together, these four bands make the data suitable for analyzing vegetation and water features. The data is acquired in the summer of 2010 and released in October 2010 [18].

Each orthophoto is divided into smaller images measuring 6.5 by 5.7 kilometers. Since the study area covers two of these images, the images were mosaiced together and clipped to match the geometry of the study area. In addition to the orthophotos, a Digital Terrain Model (DTM) with a 5-meter pixel size and 1-meter resolution in elevation was provided. DTM is a raster in which value of each pixel reports elevation of that specific area. This set of data, collected in summer of 2010, covers the entire Piedmont region.

Moreover, the line features of the main irrigation channels were supplied by the Ovest Sesia Organization of Irrigation. However, this line feature does not cover all of the channels, specially narrow ones are missed[3].

Mapping the channel network and extraction of flow direction is performed using ArcGIS Pro software, utilizing the provided orthophotos as a base. The DTM, together with the line features of the channels, was employed to determine the flow direction within the network of Channels.



Figure 2- The CIR image composing of 3 bands of Green-Red-Near Infrared

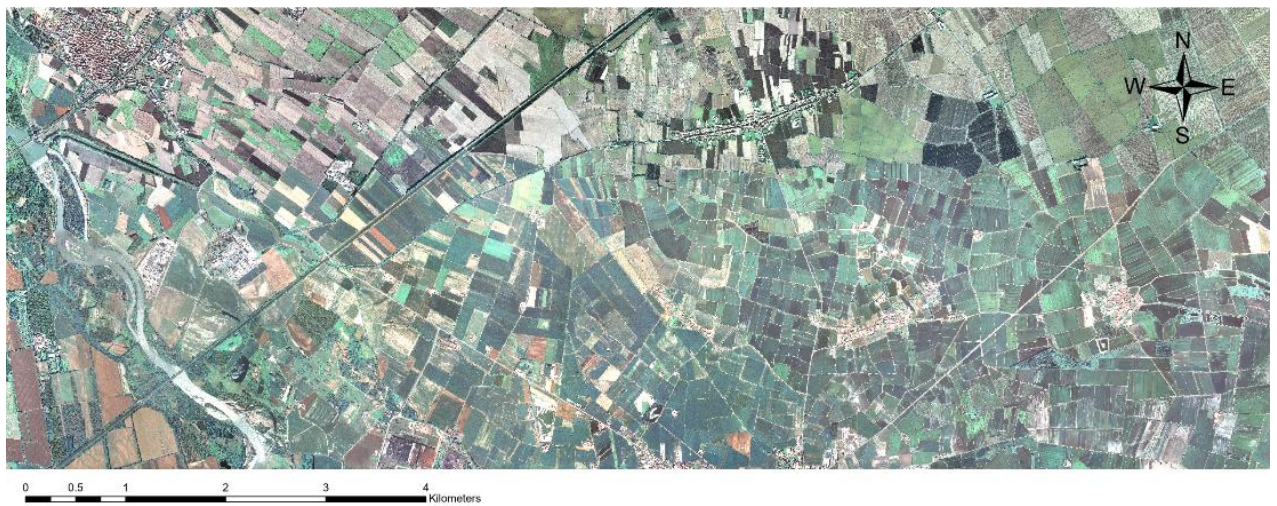


Figure 3- The RGB image composing of 3 bands of Blue-Green-Red

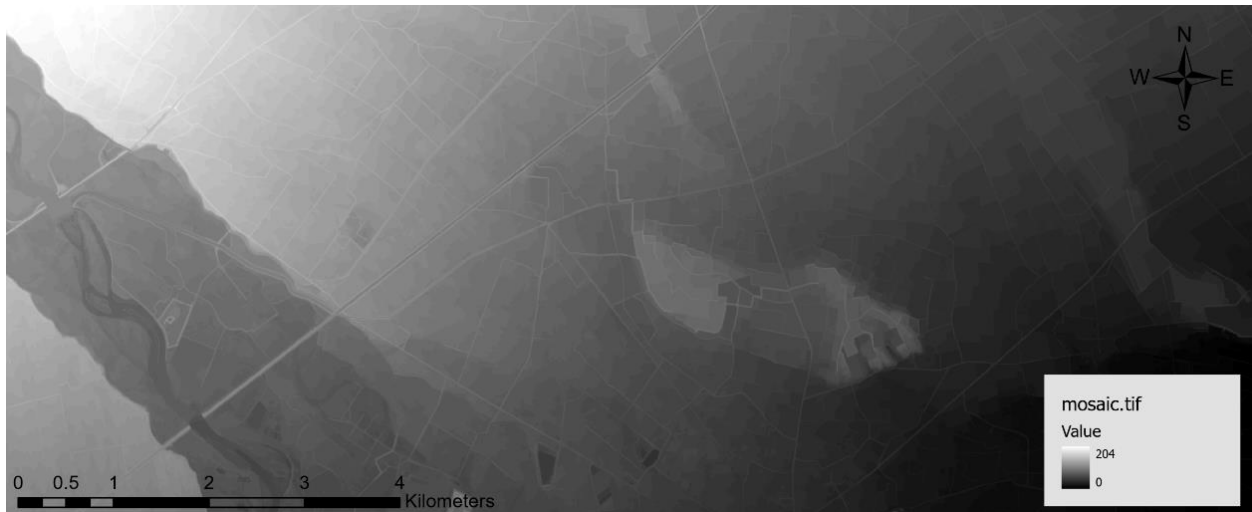


Figure 4- The Digital Elevation Model with 5 meters pixel size and 1 meter resolution in elevation, the values of elevation are reported in meter, from 0 to 204 m

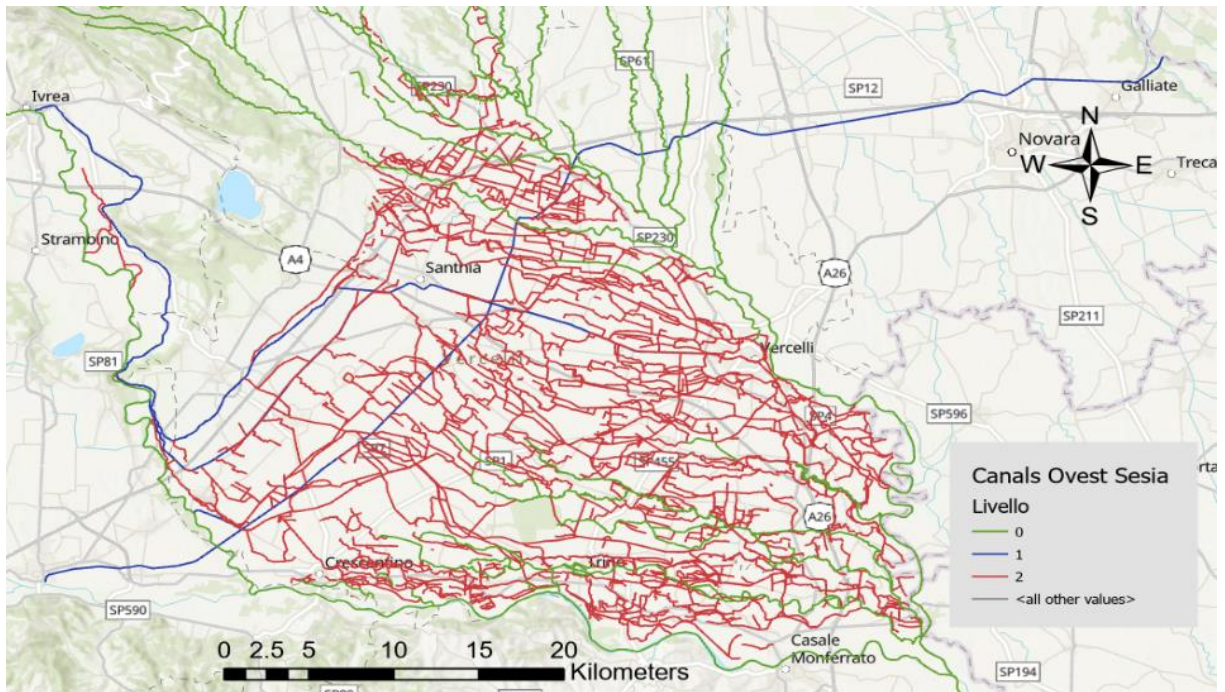


Figure 5- The line features of the channels, with 3 levels, where level 0 represents natural streams and rivers, level 1 represents the main channels like Cavour, and level 2 represents the principal irrigation channels

2.2. Role of the NIR and visible bands for water detection

The near-infrared band is highly effective for detecting water due to water's strong absorption properties in this wavelength range. Water absorbs nearly all NIR light, causing water bodies to appear as dark areas with low pixel values in NIR images. This distinct contrast between dark water surfaces and the bright reflectance of soil and vegetation in the NIR band makes it a powerful tool for identifying and mapping water-land boundaries.

In the visible range, water reflects light more strongly, particularly in the blue portion, which is most evident in clear water. Turbid water, however, has a higher reflectance in both visible and NIR regions than clear water due to suspended particles or chlorophyll, which cause scattering and increase brightness in these wavelengths.

The visible range also aids in distinguishing healthy vegetation, which absorbs blue and red light (due to chlorophyll) and reflects green, creating the green appearance of plants. Healthy plants have high reflectance in the NIR range, which varies across species due to leaf structure, allowing further discrimination among vegetation types. This contrast between high NIR reflectance from vegetation and the low NIR reflectance from water makes NIR particularly suitable for identifying water features within landscapes [19].

Figure (6) shows how the spectral signatures of clear and turbid water differ. In the NIR band, clear water is almost fully absorbing, while turbid water exhibits some reflectance due to suspended particles or dissolved substances that scatter light. This explains why, in the CIR image of the data, figure (2), rivers on the left side and in the lower half of the image show water as blue, indicating turbidity, while water in the upper parts of the image appears black, indicating greater clarity. Additionally, some sections of the river and channel appear white, which likely results from surface turbulence or foam, causing increased scattering and higher reflectance.

This variability in water reflectance can occasionally complicate the accurate distinction of water bodies, as it introduces varying spectral responses within the same image.

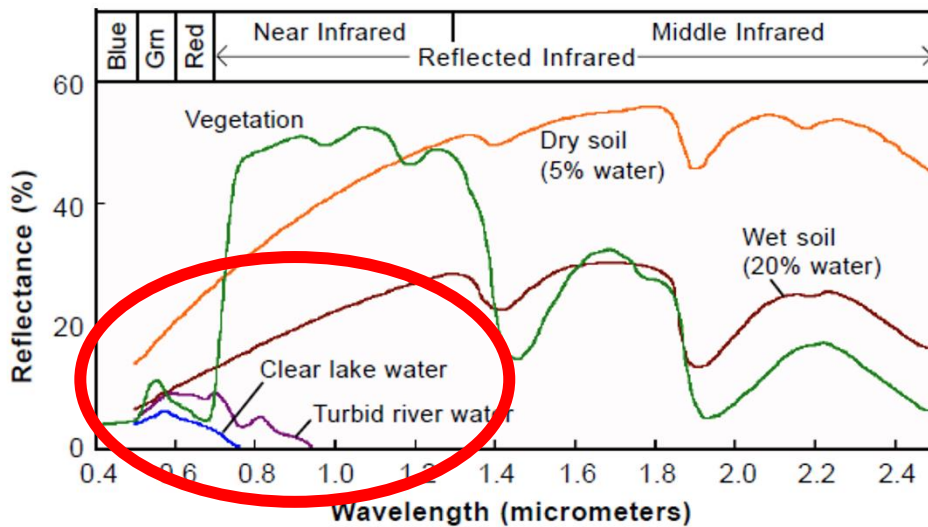


Figure 6- Signature of clear water versus turbid water , focusing on difference of reflectance of clear and turbid water

2.3. Importance of resolution of the images

When focusing on small objects such as narrow water channels, the importance of very high-resolution data with a small pixel size becomes crucial. High-resolution imagery provides greater spatial detail, allowing for more precise mapping and identification of narrow features that would otherwise be obscured or misclassified in lower-resolution images. Narrow water channels are typically only a few meters wide, so a smaller pixel size, such as sub-meter resolution, ensures that these channels are distinctly represented in the data, capturing their true shape and continuity.

With higher spatial resolution, individual pixels more accurately reflect the specific characteristics of narrow channels, improving the ability to differentiate them from surrounding land features like soil or vegetation. This level of detail is particularly beneficial for automated classification and flow analysis, reducing errors in detecting channel boundaries and enhancing the accuracy of water flow models. Consequently, high-resolution imagery enables better monitoring, management, and maintenance of irrigation networks, making it invaluable for agricultural and water resource applications.

2.4. Importance of resolution of DTM data

The resolution of Digital Terrain Model (DTM) data is critically important for accurately extracting flow direction within narrow water channels. Fine elevation resolution enhances the DTM's ability to detect tiny changes in terrain elevation that govern the flow gradient. Small variations in channel depth or slope, which are crucial for determining flow direction, can be missed or smoothed out in low-resolution DTMs, leading to inaccurate flow analysis. High-resolution DTMs provide the detailed topographical data needed to calculate precise flow directions, ensuring that water movement within channels is modeled as realistically as possible. This level of detail is essential for effective water management, flood prediction, and irrigation planning in areas with complex or narrow channel networks.

3. Methods and results

3.1. Methodology

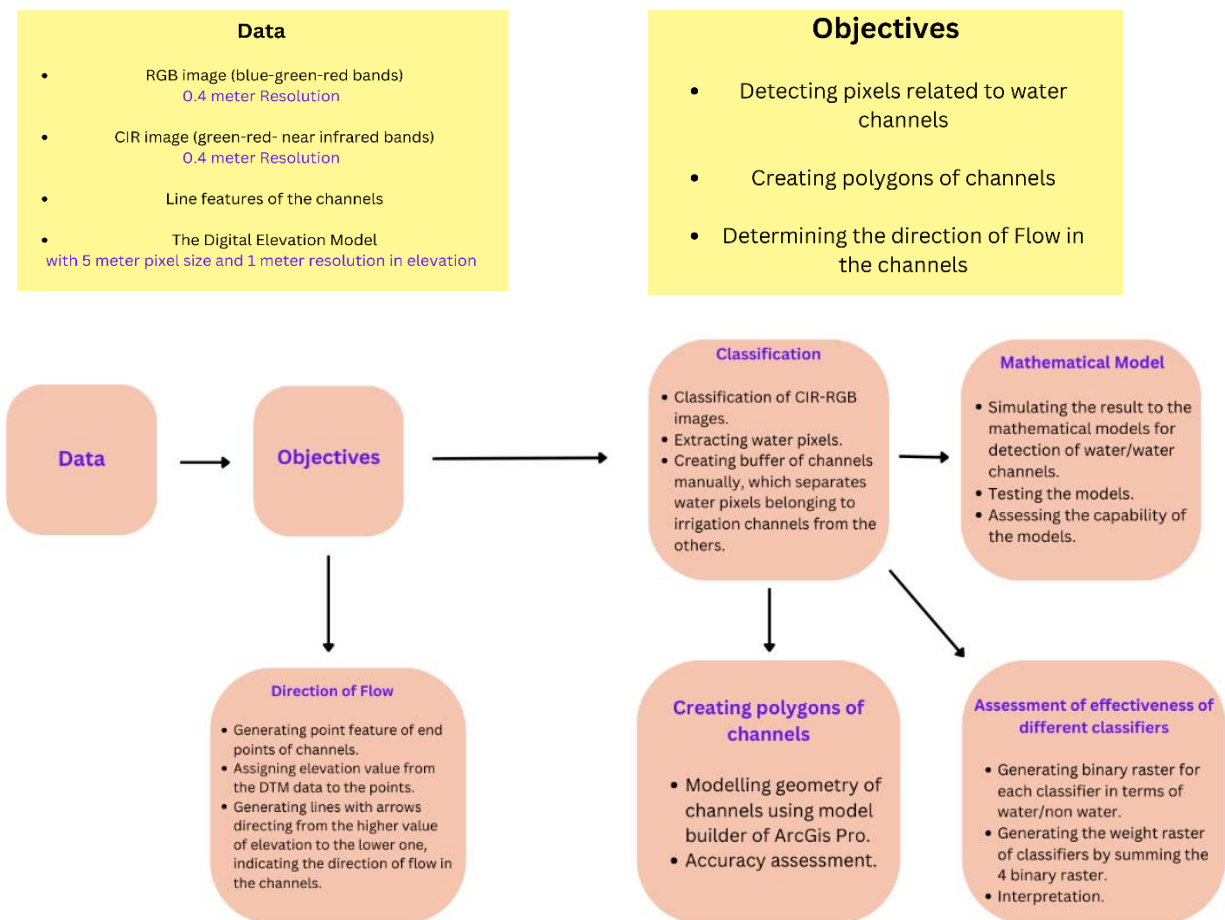


Figure 7- Graphical workflow of methodology

In order to detect water pixels and separate them from other surfaces, the first step is to classify the image.

Image classification is a technique used to group and label parts of an image, based on certain rules, by analyzing collections of pixels or vector data within the image. This process allows for identifying specific elements in an image by using different characteristics, such as color (spectral) or texture. These distinguishing features help to categorize different regions in the image effectively.

There are two primary approaches to image classification: unsupervised classification and supervised classification.

Unsupervised Classification: In unsupervised classification, the image classification process is entirely automated, meaning no prior examples or labeled data are needed. Here, the computer independently identifies patterns and groups within the image based on certain characteristics, without any human input. This is achieved through specialized algorithms that systematically detect clusters or similarities among pixels. Since this method doesn't require training data, it can be highly efficient, especially for analyzing large datasets, as it rapidly detects categories based solely on statistical patterns in the image.

Supervised Classification: In contrast, supervised classification involves using labeled samples, or "training data," selected from specific areas within the image to guide the classification process. These sample areas are chosen by a human and assigned to predefined categories, such as "roads," "buildings," "water bodies," or "vegetation." By using these labeled samples, the computer can develop statistical measures and patterns associated with each category, which it then applies to classify the rest of the image. Supervised classification typically relies on statistical models, such as maximum likelihood and random forest algorithms, to analyze and categorize the entire image based on the training data. These methods are powerful as they use existing knowledge to improve the accuracy and relevance of the classification, making supervised classification highly effective for tasks where specific, well-defined categories are needed[20].

This study has made use of supervised classification methods. This step together with all the other geospatial analyses are performed in ArcGIS Pro software.

3.1.1. The choice of supervised classification with respect to the unsupervised approach

For detection of specific narrow objects like water channels, supervised classification often proves more effective than unsupervised methods because it allows us to precisely identify and label examples of the target feature in the image, which guides the algorithm in recognizing similar features across the entire image.

1.Improved Feature Recognition in Complex Environments: Supervised classification provides higher accuracy and enhanced feature recognition when identifying targeted classes, such as specific natural features like water channels. By using labeled training data, the algorithm is able to focus on distinguishing well-defined objects based on their unique spectral or textural characteristics. This is particularly advantageous in complex environments where water channels are surrounded by similar features, such as vegetation or soil. Unlike unsupervised classification, which may group similar-looking features due to the lack of training guidance, supervised classification effectively "teaches" the algorithm to recognize and separate these targeted features with greater precision[21].

2.Flexibility with Complex Class Definitions: Supervised methods provide flexibility in defining complex classes that may not emerge naturally through statistical clustering, as in unsupervised methods. Narrow water channels, in particular, may have spectral characteristics that only slightly differ from their surroundings, making them difficult to isolate without explicit guidance. Supervised classification, especially when using advanced methods like the Random Forest algorithm, enables the system to use multiple sample points and a combination of features to distinguish water channels effectively[22].

3.Greater Control over the Classification Process: Supervised classification also allows users to apply domain knowledge, setting up specific categories based on known characteristics of the water channels. This improves precision and ensures that the classification is both accurate and meaningful in real-world applications where certain features need to be reliably separated for analysis [23].

3.1.2. Supervised pixel-based classification for water detection

For detecting water, researchers often use specialized water indices like the Modified Normalized Difference Water Index (MNDWI), Normalized Difference Moisture Index (NDMI), or Automated Water Extraction Index (AWEI). These indices rely on band calculations that typically include Short-Wave Infrared (SWIR) bands, which capture water absorption features at wavelengths of 1.4, 1.9, and 2.7 μm [24]. However, this study is limited to four bands—Red, Green, Blue (RGB), and Near-Infrared (NIR)—which restricts the use of indices that require SWIR bands. As a result, supervised classification is chosen as an alternative approach for water detection. In agricultural landscapes, detecting water channels presents additional challenges due to their narrow, irregular boundaries. These characteristics often lead to weak responses in morphological operations, such as those used in Digital Morphological Profiles (DMPs), which are more effective for detecting defined, continuous shapes like rivers or buildings [25]. The small size and irregular shape of water channels can result in inaccurate classification, as they do not maintain consistent structural properties.

Moreover, agricultural fields typically exhibit complex land cover patterns, mixing crops, irrigation infrastructure, soil, and water bodies. This diversity introduces significant noise in object-based classification methods, which focus more on structural aspects than on moisture content, reflectivity, or other spectral factors critical for detecting water. Therefore, integrating supervised classification techniques is essential for accurately identifying and differentiating water bodies within such intricate agricultural environments.

3.2. Workflow

3.2.1. First level classification: CIR image



Figure 8- The CIR image, input data of the first level classification

The CIR image consists of three spectral bands: Near-Infrared (NIR), red, and green. A supervised classification was performed to extract water pixels, with training samples (polygons) collected from across the entire image. To create the training sample file, the Training Samples Manager pane is used which is of the Classification Tools of imagery section . The classification is performed by defining four classes:

- 0 : Water
- 1 : Green, healthy vegetation
- 2 : Harvested vegetation, which is composed of a mixture of soil and dryer vegetation
- 3 : Built areas, which include cities and roads

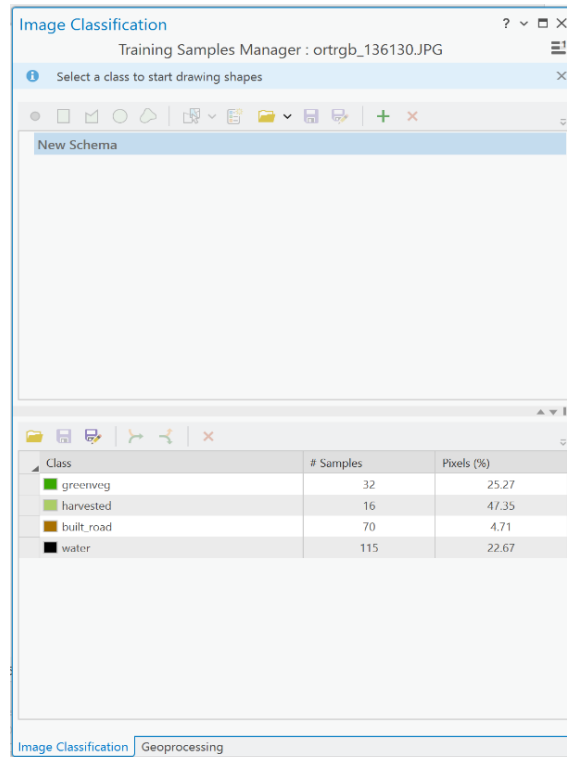


Figure 9- Generating the shape file of the training samples using the tool of "Training sample Manager"

When extracting training samples of built areas, it is tried to avoid selecting vegetation within urban areas. Green vegetation includes forests, vegetation in cities, and agricultural fields that appear green. In contrast, agricultural fields affected by harvesting, where crops have been removed and there is some influence of soil or woody materials in the reflectance, are grouped under harvested vegetation.

The classification process was carried out using four classifiers available in ArcGIS Pro:

- K-Nearest Neighbor
- Random Trees
- Support Vector Machine (SVM)
- Maximum Likelihood

K-Nearest neighbor classifier

The K-Nearest Neighbor classifier is a nonparametric classification method that classifies a pixel or segment by a plurality vote of its neighbors. K is the defined number of neighbors used in voting.

The tool assigns training samples to their respective classes. The class of the input pixel is determined by a plurality vote of its K-nearest neighbors. The classification is performed with $K = 1$ [26].

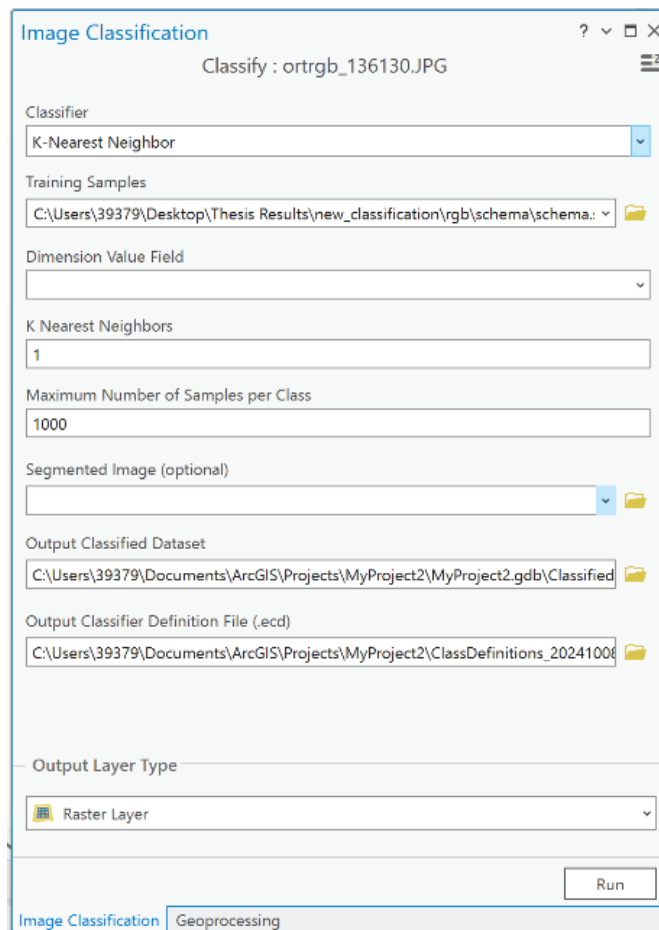


Figure 10- The K-nearest neighbor classifier

Random trees

The Random Trees classifier is a supervised image classification method that reduces overfitting by using a collection (or "forest") of decision trees. Each tree is constructed from different random samples and subsets of the training data. For each pixel (or segment) in an image, multiple decision trees make predictions, and the final classification is determined by the majority vote across trees. This method introduces randomness by selecting different subsets of variables for each tree, which helps avoid overfitting the training data. The classifier supports multiband imagery with various bit depths, making it flexible for diverse image data [27].

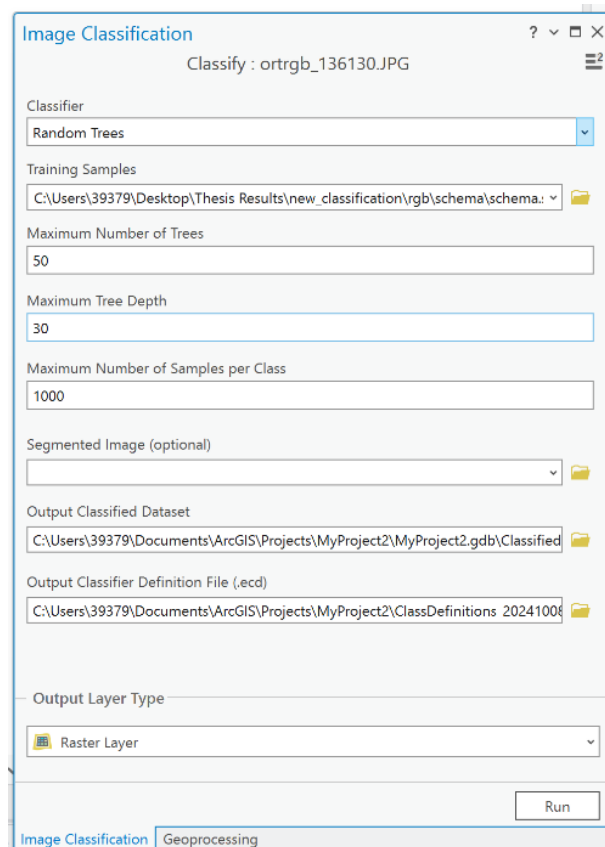


Figure 11- The random trees classifier

SVM

The SVM (support vector machine) classifier is a supervised classification technique aimed at identifying the best boundary, known as a hyperplane, to effectively separate data points belonging to different classes. It is compatible with standard image inputs, allowing for multiband image, and it applies SVM classification on a pixel-by-pixel basis using an input training feature file. The SVM method requires fewer training samples and does not assume that the samples follow a normal distribution[28].

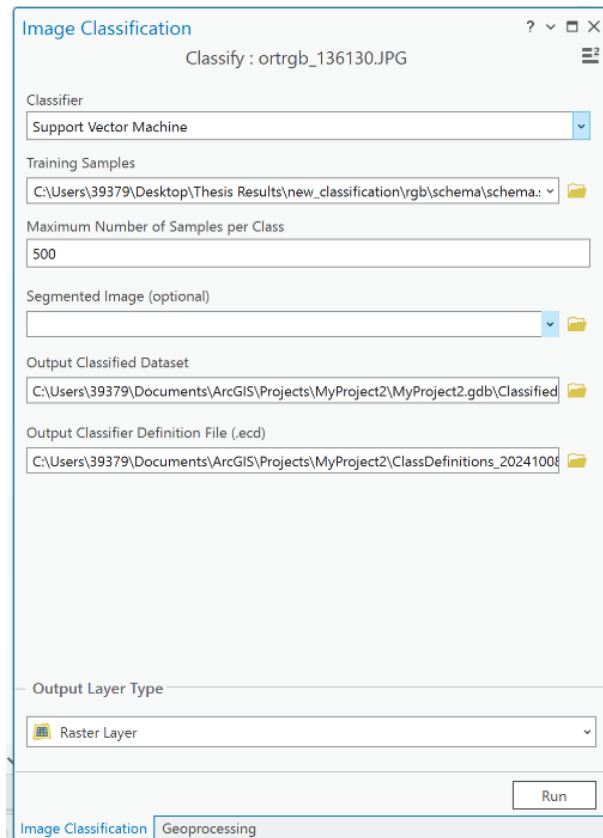


Figure 12- The support vector machine classifier

Maximum likelihood

Maximum likelihood classification uses the statistical properties of the data by first calculating the mean and standard deviation for each spectral and textural index in the image. Assuming a normal distribution of pixels within each class, it then uses statistical and probabilistic methods to estimate the likelihood of each pixel belonging to each class. Each pixel is ultimately assigned to the class for which it has the highest likelihood[29].

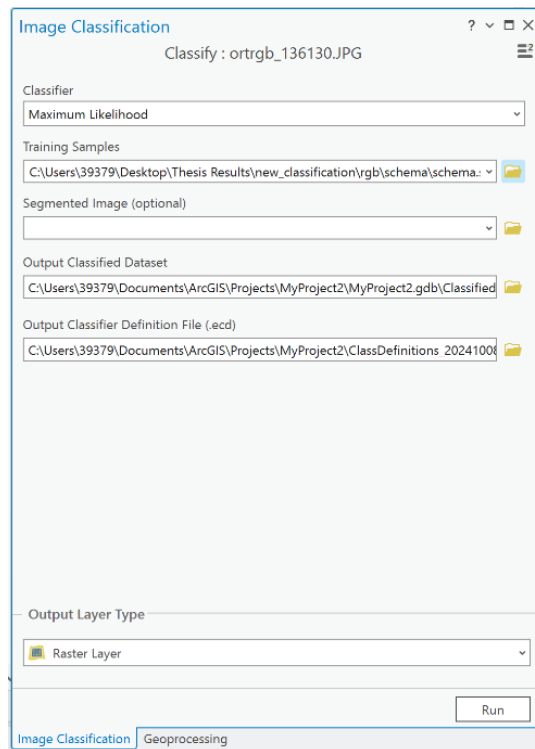


Figure 13- The maximum likelihood Classifier

Results

Each classifier produced a classified raster image, each with one band and four values, corresponding to the four classes reported in the figures below.

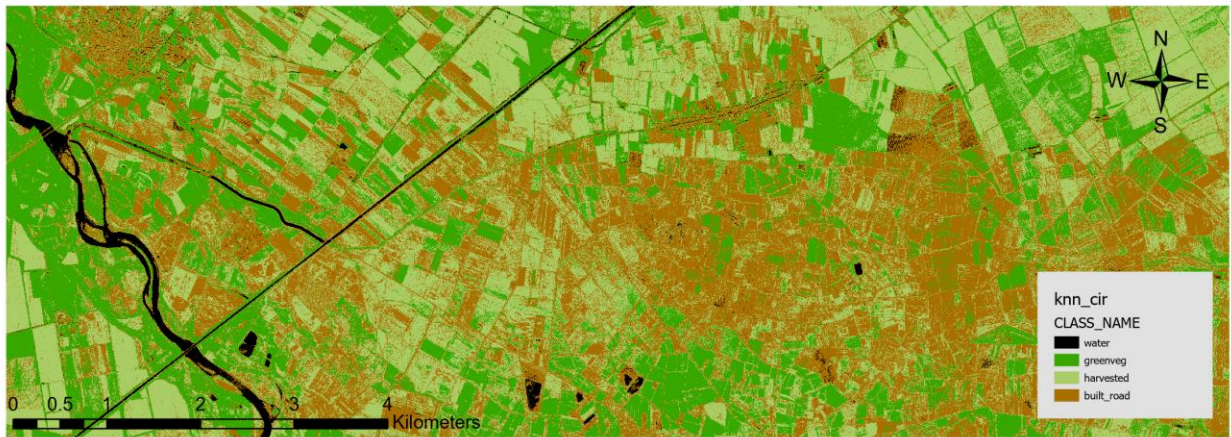


Figure 14- The classified raster of K nearest neighbor

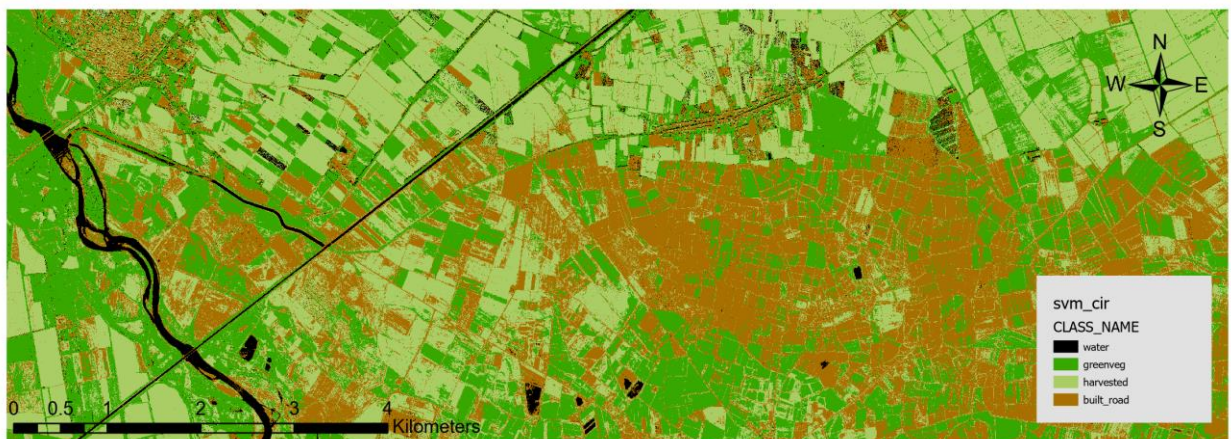


Figure 15- The classified raster of SVM

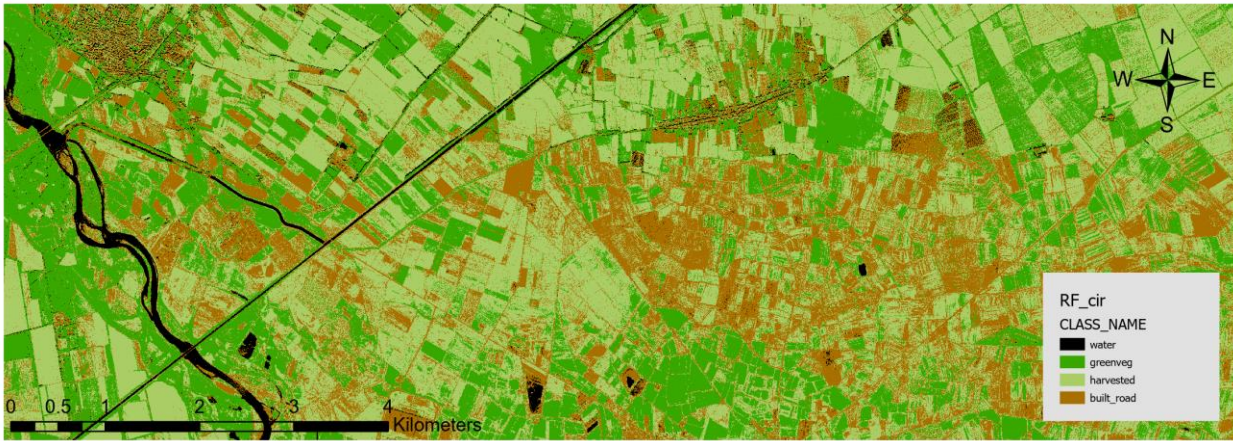


Figure 16- The classified raster of random trees

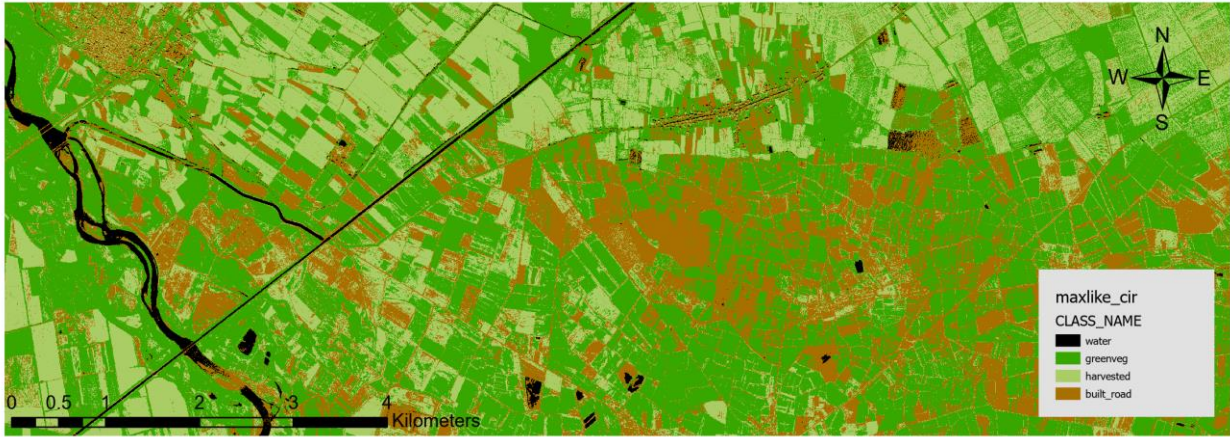


Figure 17- The classified raster of maximum likelihood

Next, the pixels marked as water by every classifier are separated and extracted. By “select by attribute” tool, only the class of water is selected and a from that selection new layer is generated.

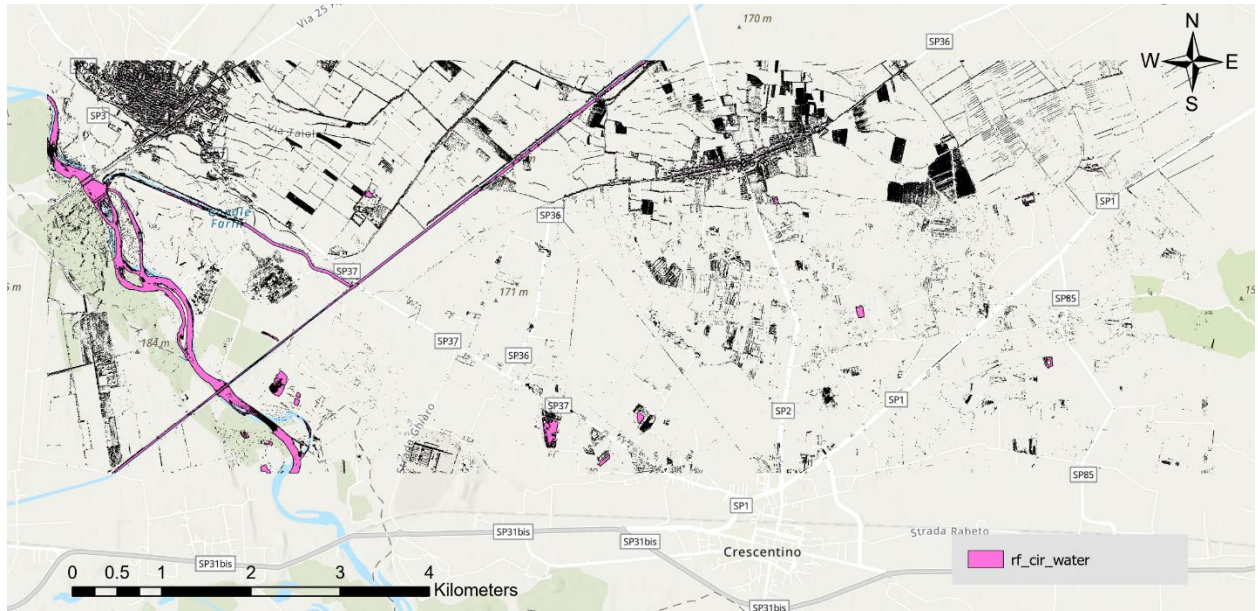


Figure 18- Water pixels resulting from the random trees classifier

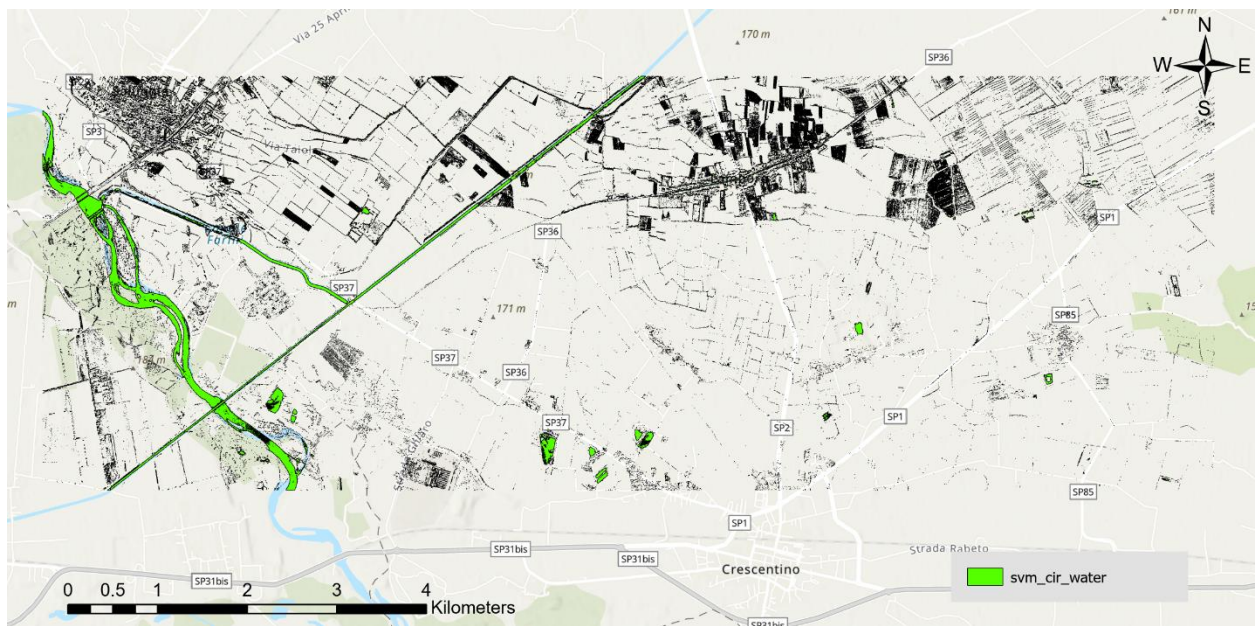


Figure 19- Water pixels resulting from the support vector machine classifier

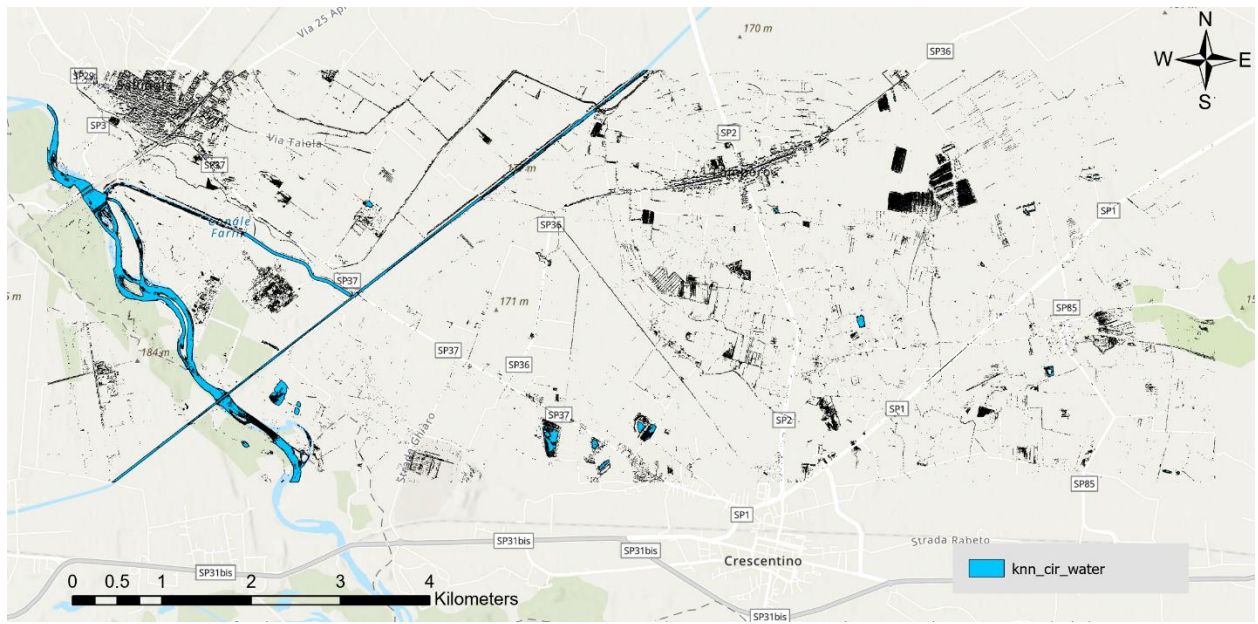


Figure 20- Water pixels resulting from the K nearest neighbor classifier

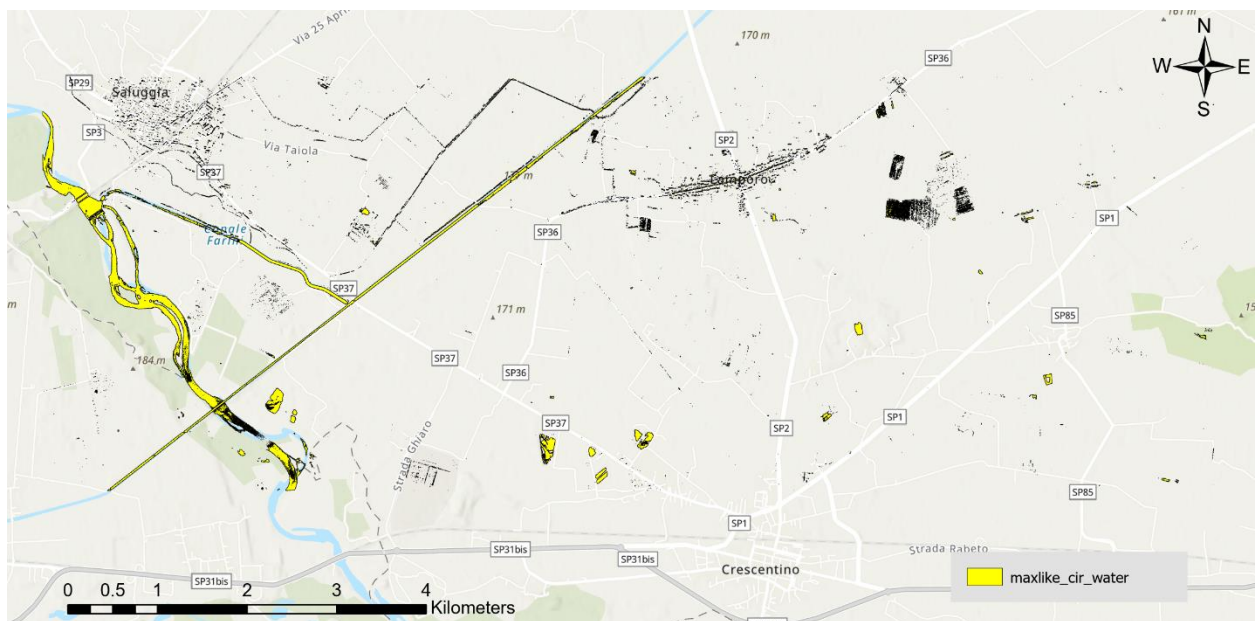


Figure 21- Water pixels resulting from the maximum likelihood classifier

However, as water pixels in the channels were highly scattered due to the small size of the channels relative to the geometric resolution of the image, the water polygons from all four classifiers were aggregated to maximize the capture of water pixels. This aggregation was performed using the "merge" tool.

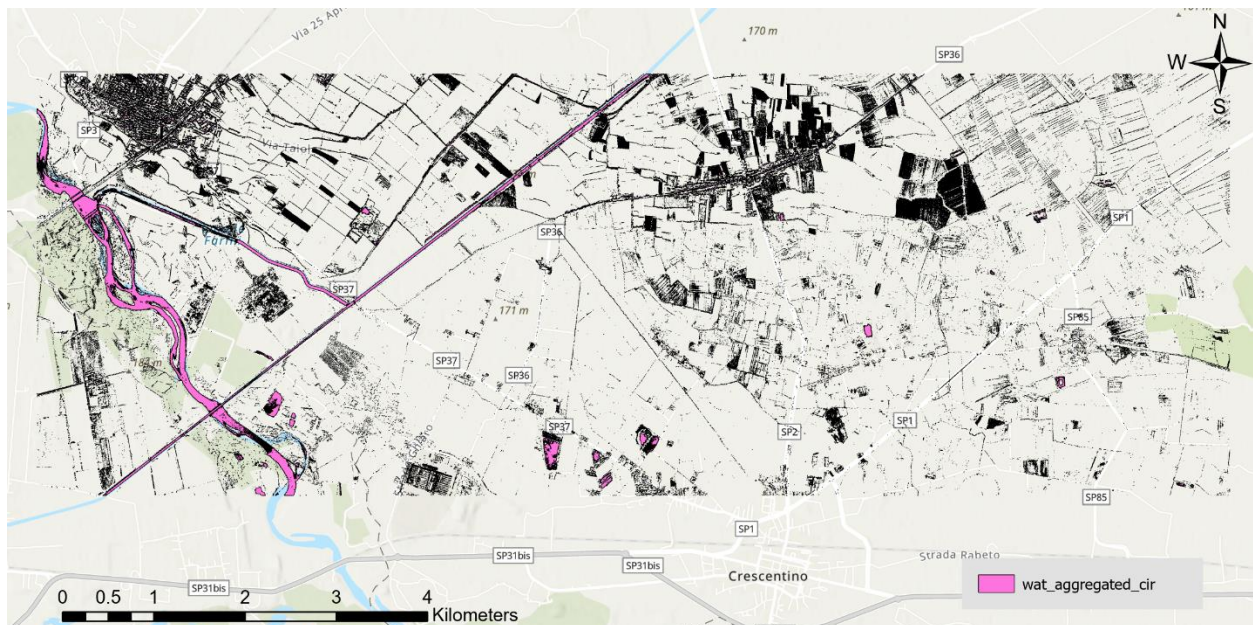


Figure 22- Water polygons aggregated from all of the four classifiers performed in the first level of classification

Since some pixels marked as water were actually shadows or roads due to their similar reflectance in parts of the image (False positive, error type I), a subsequent classification is conducted using the RGB image to further differentiate and separate true water channel pixels from those misclassified as water which are actually roads or shadows.

The water pixels detected in the classification of the CIR image, serve as input for the next stage, which involves in classifying the RGB image. For this purpose, the RGB image is masked by the aggregated water pixels of the first CIR classification (figure22) using the tool of "Extract by Mask", which is the input of the next level classifier.

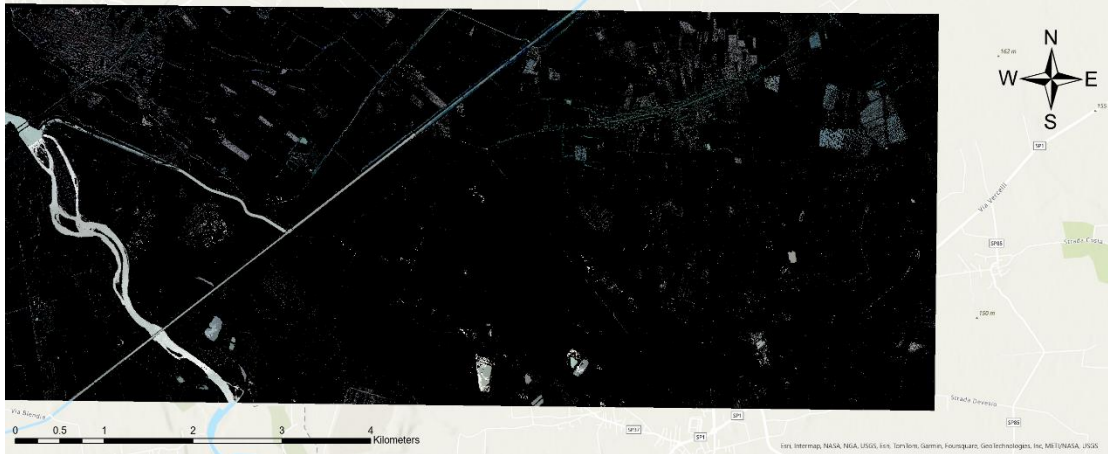


Figure 23- The RGB image masked by the aggregated water polygons of figure 21, which is input of the second level classification

3.2.2. Second level classification: RGB Image

This classification is also supervised, with training sample polygons assigned to four classes:

- 0: Water
- 1: Road
- 2: Shadow
- 3: Masked areas, which are those areas detected as “non-water” in the previous classification and are in black in figure 22.

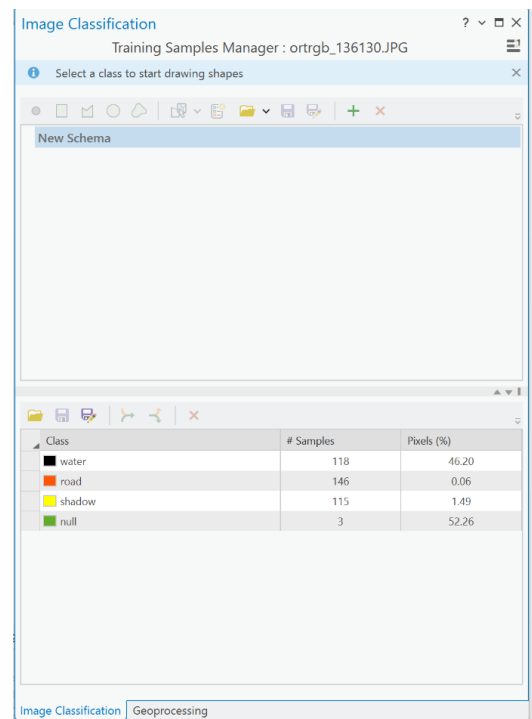


Figure 24- Training samples of the second level classification

The classification process was similarly conducted using the same four classifiers as in the previous step: Nearest Neighbor, Random Trees, Support Vector Machine, and Maximum Likelihood. As with the first level classification, the scattered nature of the water pixels meant that instead of selecting the best-performing classifier, the results from all four classifiers were aggregated.

The RGB classification successfully separated water pixels from road pixels to a satisfactory degree. However, it still encountered difficulties in fully differentiating between water and shadow which is the result of similarity of reflectance of shadow and water in the four bands of RGB, NIR. As a result, the water polygons from this step include not only actual water pixels but also shadow and a very small amount of road pixels. Additionally, these water polygons include various water features, such as water bodies like lakes and rivers, and irrigation-flooded fields. Below is the results of RGB image classification for the four classifiers.

Results

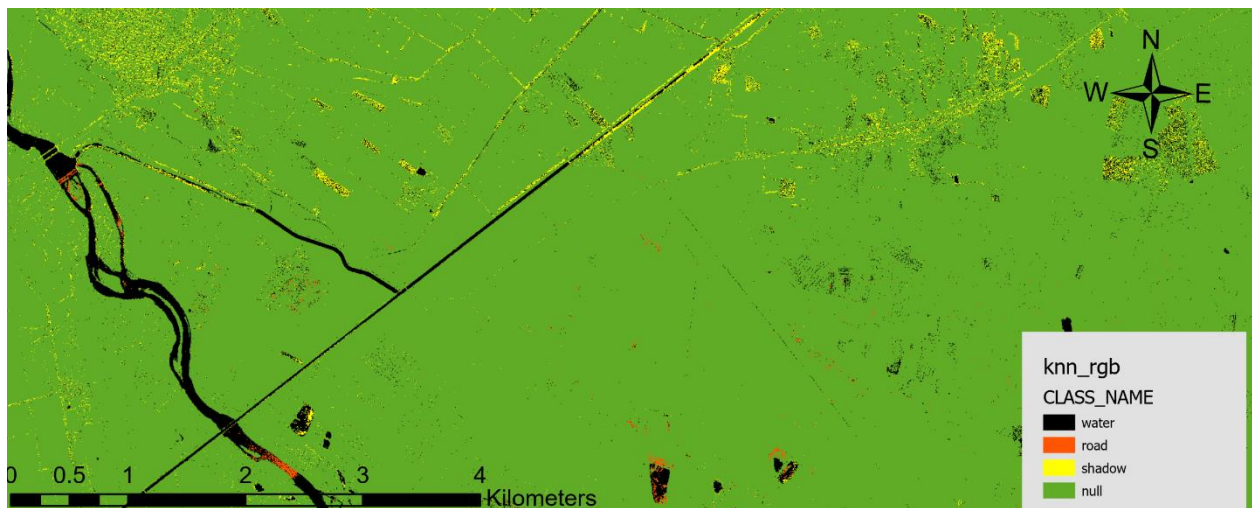


Figure 25- The second level classified raster of the K-nearest neighbor classifier

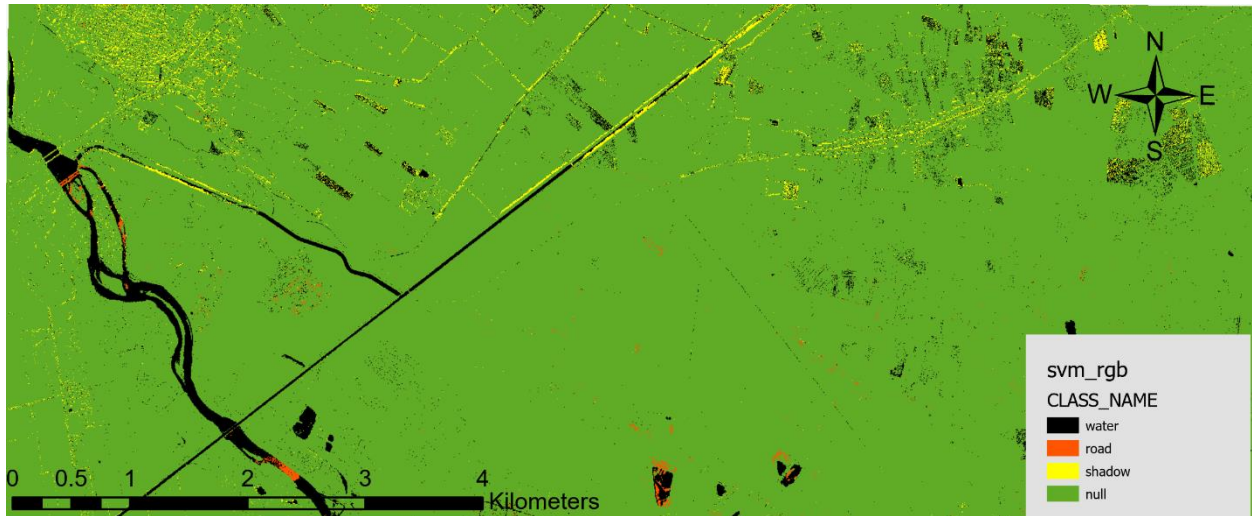


Figure 26- The second level classified raster of the SVM classifier

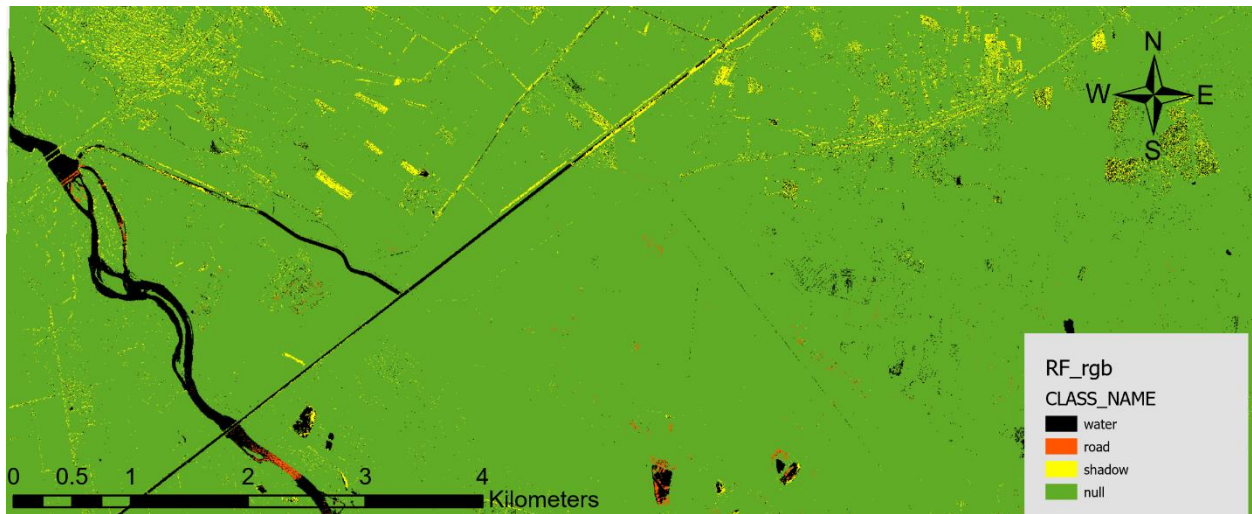


Figure 27- The second level classified raster of the random trees classifier

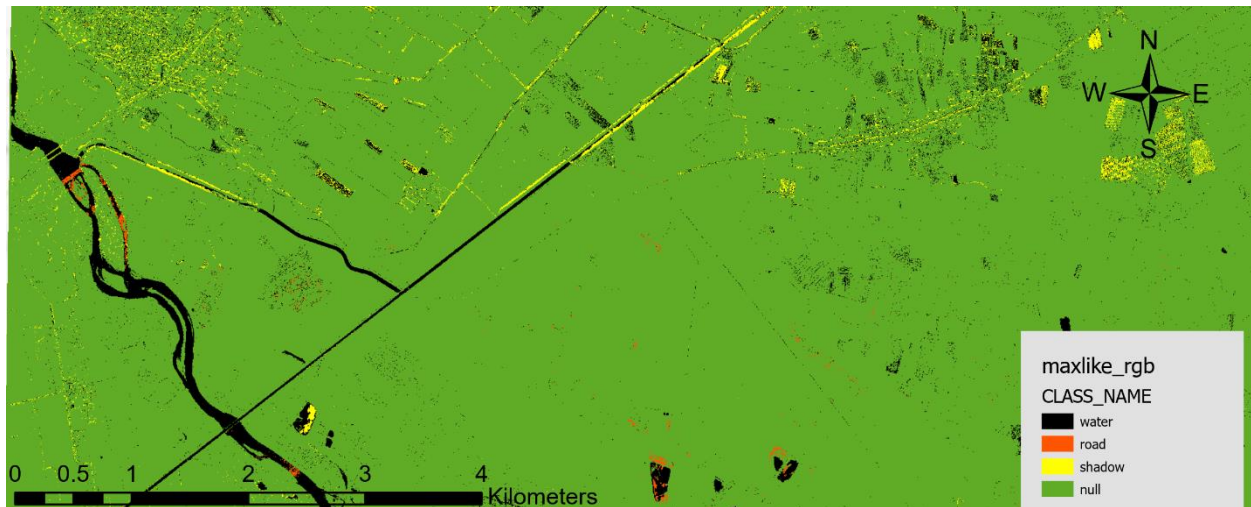


Figure 28- The second level classified raster of the maximum likelihood classifier

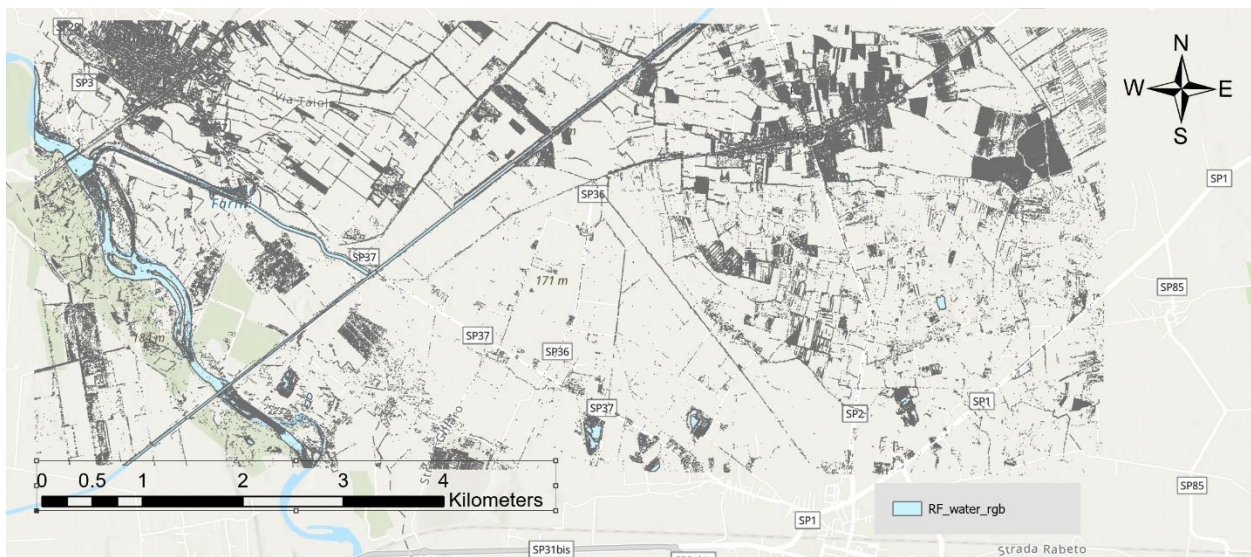


Figure 29- Water pixels resulting from the random forest classifier of the second level

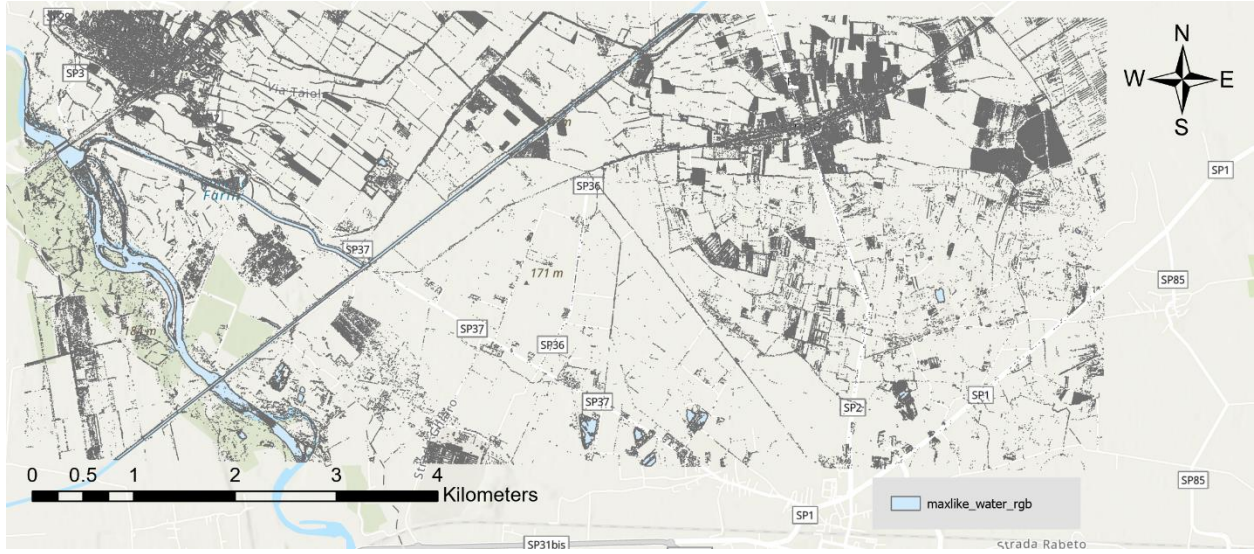


Figure 30- Water pixels resulting from the maximum likelihood classifier of the second level

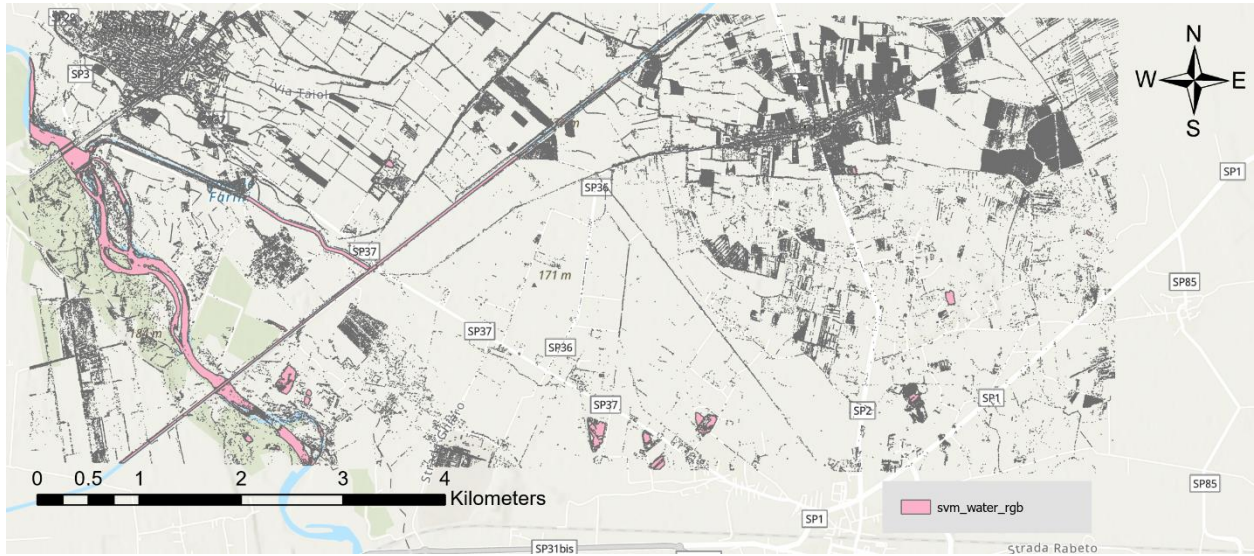


Figure 31- Water pixels resulting from the SVM classifier of the second level

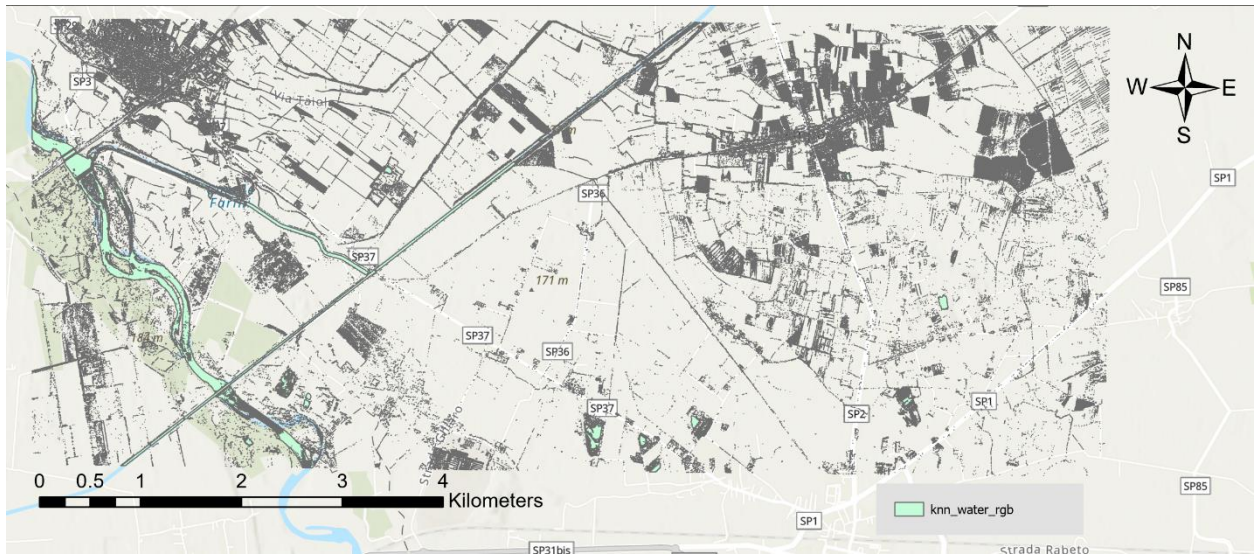


Figure 32- Water pixels resulting from the K-nn classifier of the second level

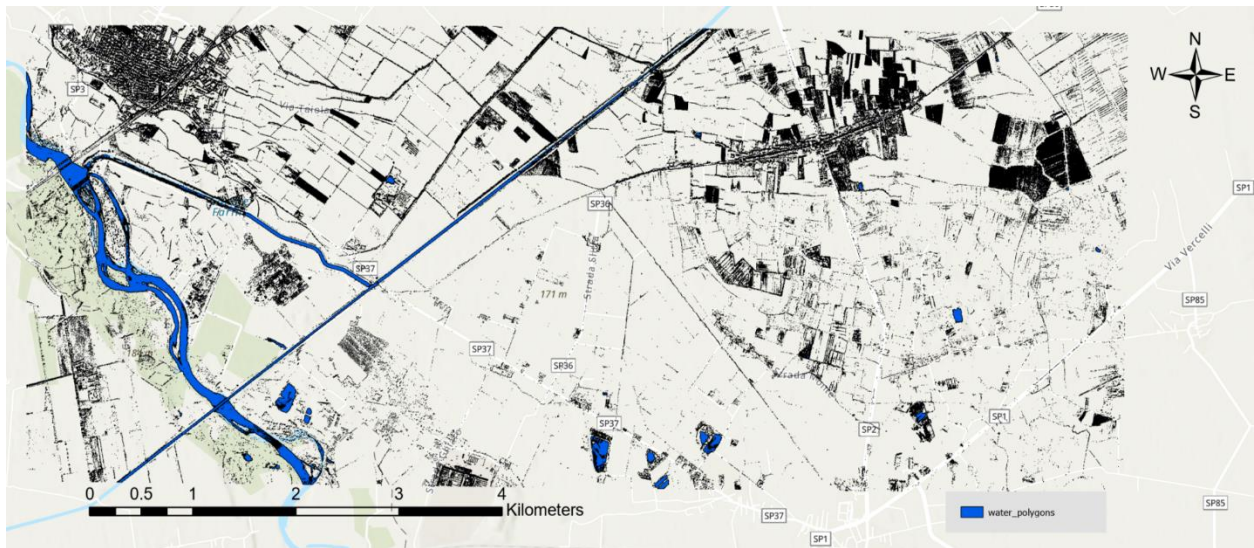


Figure 33- Water polygons aggregated from all of the four classifiers performed in the second level of classification, which is considered as the final result of water pixels from the classification step

3.2.3. Creation of buffers for channels

Since the aim is to map only the water within the channels, it is necessary to separate the water pixels associated with the channels from other water pixels. To achieve this, a buffer is created around each segment of the channel. The buffer should be created in a way that encompasses all the water polygons relevant to each part of the channel while excluding any unwanted polygons from other areas, including shadow of nearby trees, or other water pixels that do not belong to channels.

For a smaller subset within the study area (in pink in the figure 33), channel buffers are manually created using "Create Feature Class" for all the channels in the subset. These buffers are generated to ensure that all water polygons belonging to each section of the channel are aligned in a straight line, so when the direction of the channels is meandering, the buffer is divided into 2 on the spot that direction changes, in a way that finally every polygon have shape of a long rectangle. The main RGB and CIR orthophotos are used as a base map to verify that these polygons indeed represent water channels. This subset, with a quasi-triangular shape, is located between the cities of Crescentino and Saluggia, northeast of Torino, covering an area of approximately 19.8 square kilometers, with the center located at coordinates [8.076 east, 45.215 north]. (Figure 33).

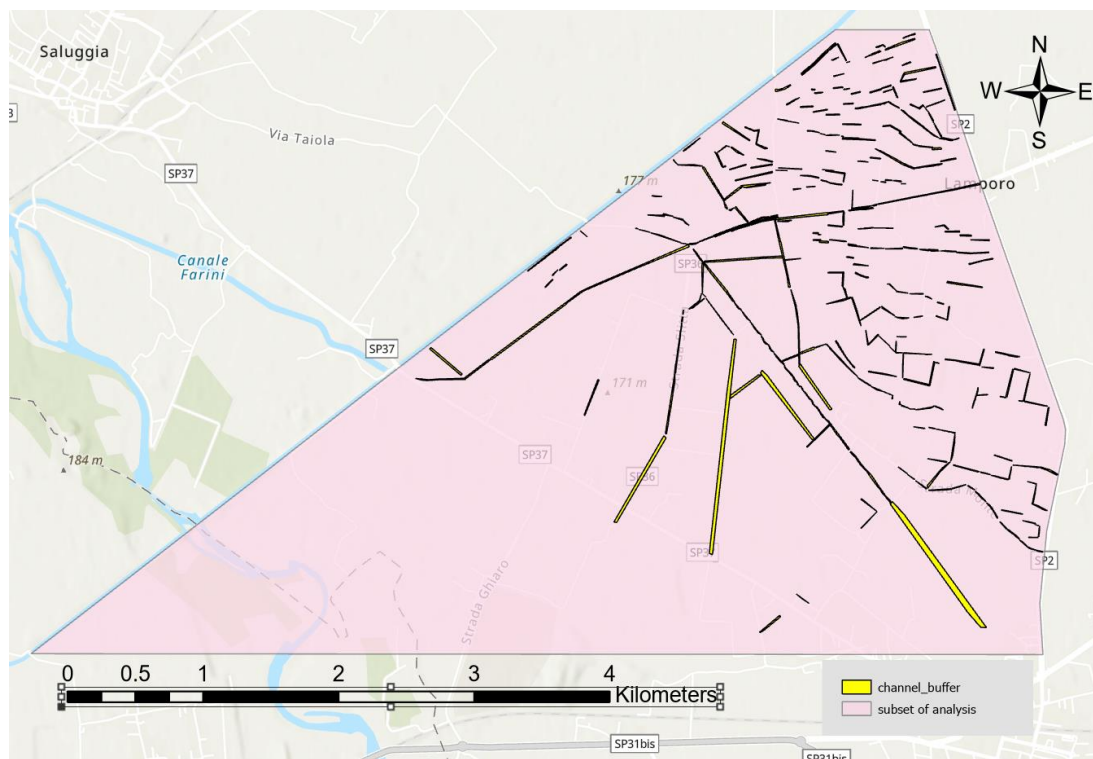


Figure 34- The buffers of the channels



Figure 35- The buffer of one segment channel holds all the water polygons related to that segment of the channel

The purpose of creating channels buffers, besides excluding unwanted polygons marked as water, is to group the water polygons within each channel section to facilitate the creation of the channel geometry. The manual buffer creation for the study subset took around 10 hours, resulting in 337 polygons.

3.2.4. Evaluation of performance of each classifier

Method

In order to evaluate the performance of each classifier, the binary raster of result of water detected by each classifier is generated with values of 0 representing non-water and values of 1 representing water.

This step is conducted on the first level classification which is performed on the CIR image, because it takes advantage of the two most effective bands for water detection which are red and NIR and is performed on the full subset of the image. The binary rasters are generated using the tool of “con”.

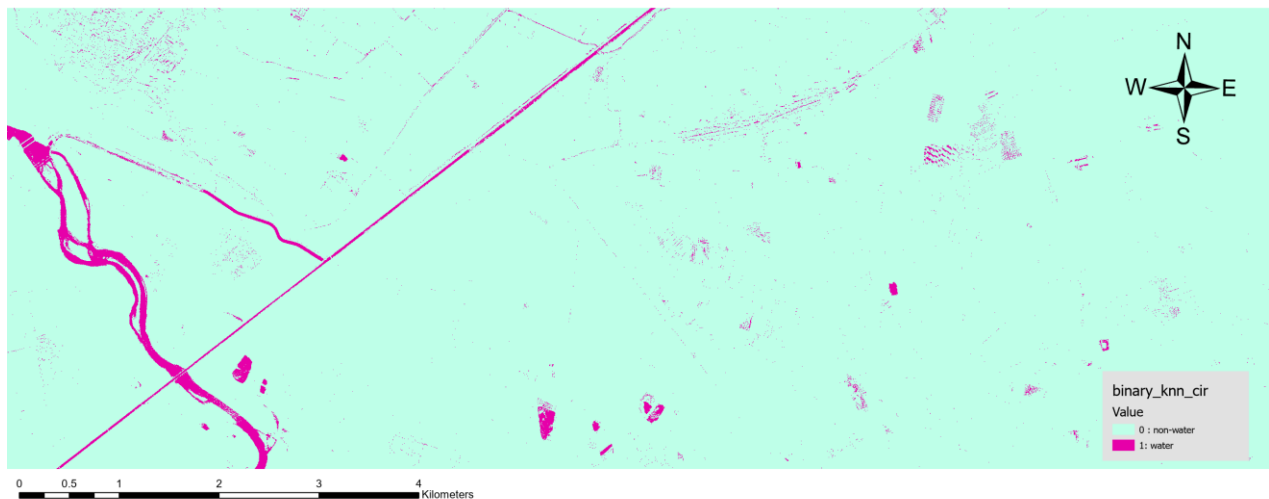


Figure 36- The binary raster of water and non-water of K nearest neighbor classifier

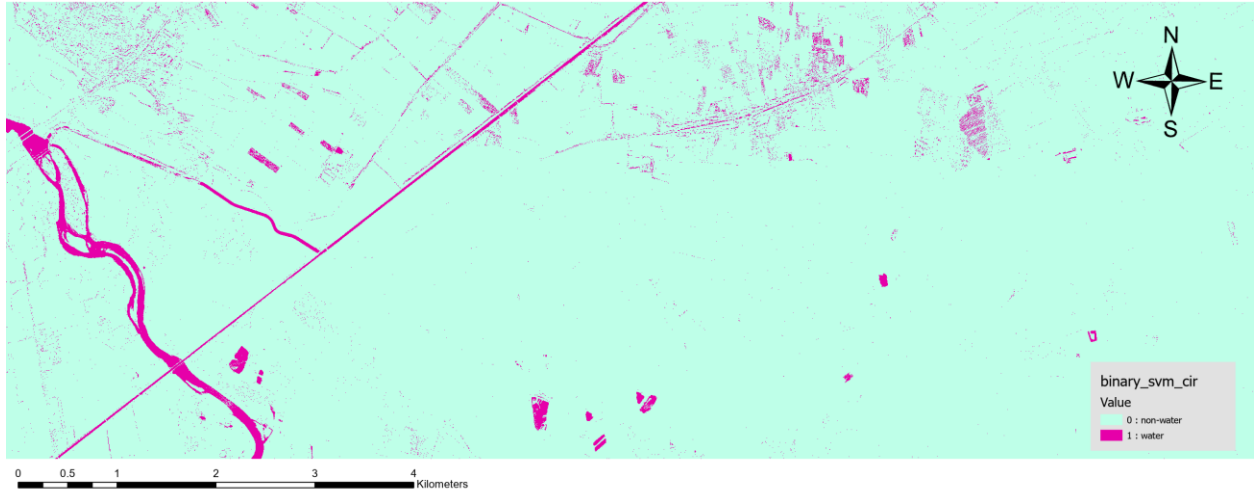


Figure 37- The binary raster of water and non-water of SVM classifier

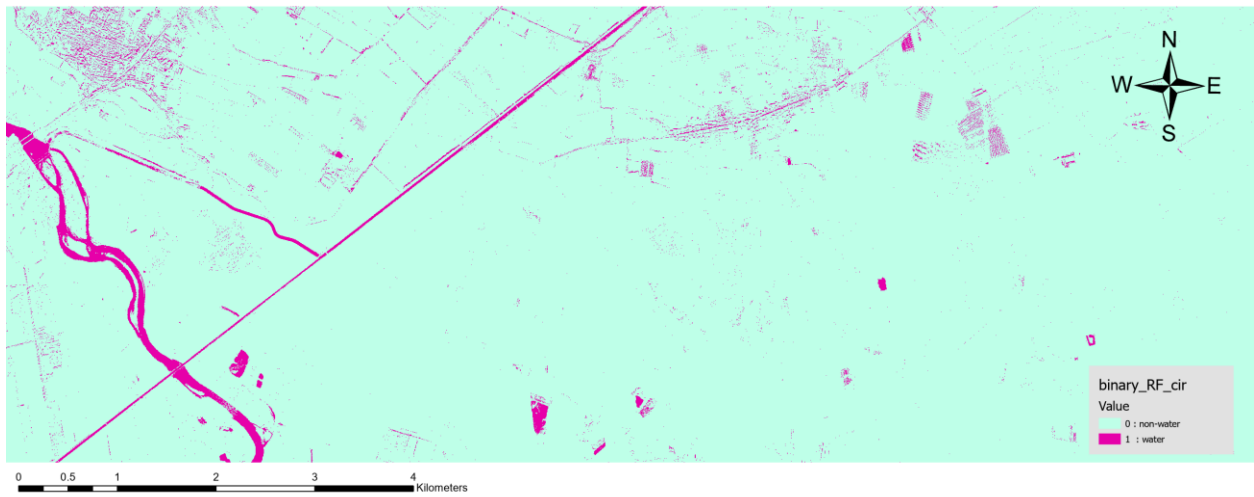


Figure 38- The binary raster of water and non-water of random trees classifier

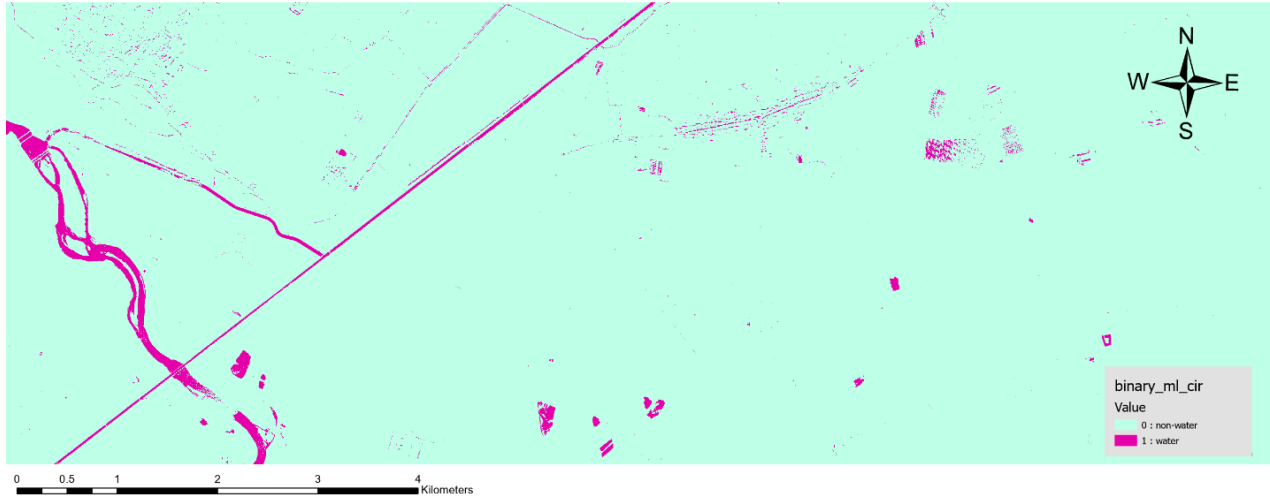


Figure 39- The binary raster of water and non-water of maximum likelihood classifier

Then the four binary rasters are summed to build a weight raster with values of 0 to 4, where 0 represents “non-water”, 1 represents “pixels detected as water by 1 classifier”, up to 4 that represents “pixels detected as water by all of the 4 classifiers”. The summation step is performed using the tool of “Calculate Field”.

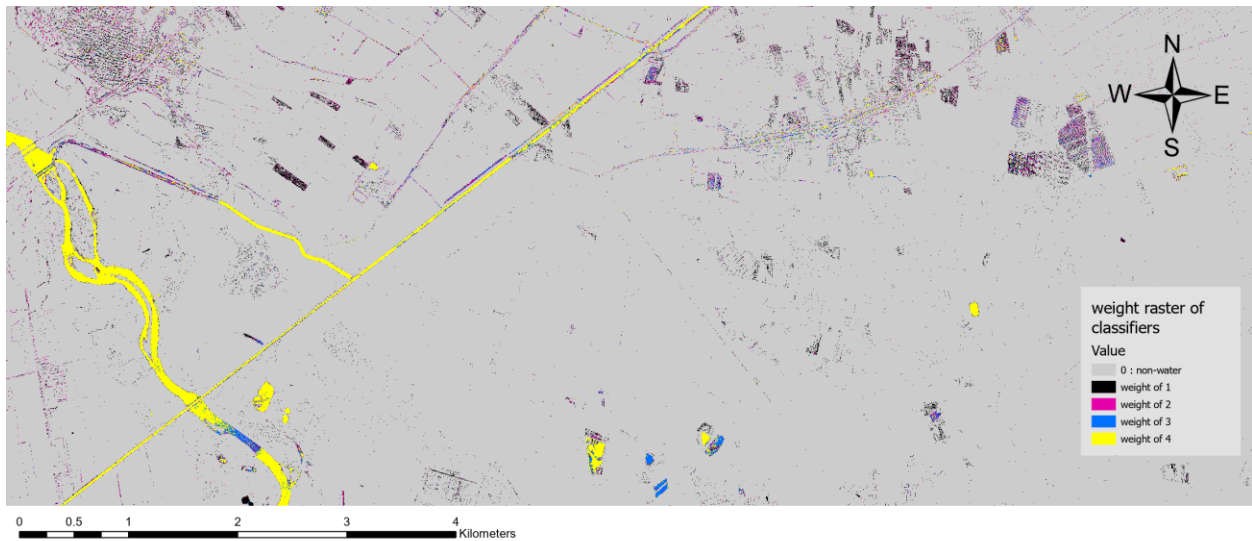


Figure 40- The Weight raster of classifiers, which is the sum of the four binary rasters

Focusing on the weight raster, the weight of 4 represents majorly indicated water bodies like lakes and rivers. This means they are marked as water by all the 4 classifiers, while pixels related to finer water channels have weights of 1 or 2, as they have mostly mixed and edging pixels rather than pure pixels of water.

To understand which classifier works better for detection of finer water channels, the weight raster as well as the four binary rasters are extracted by mask of the channels buffers.

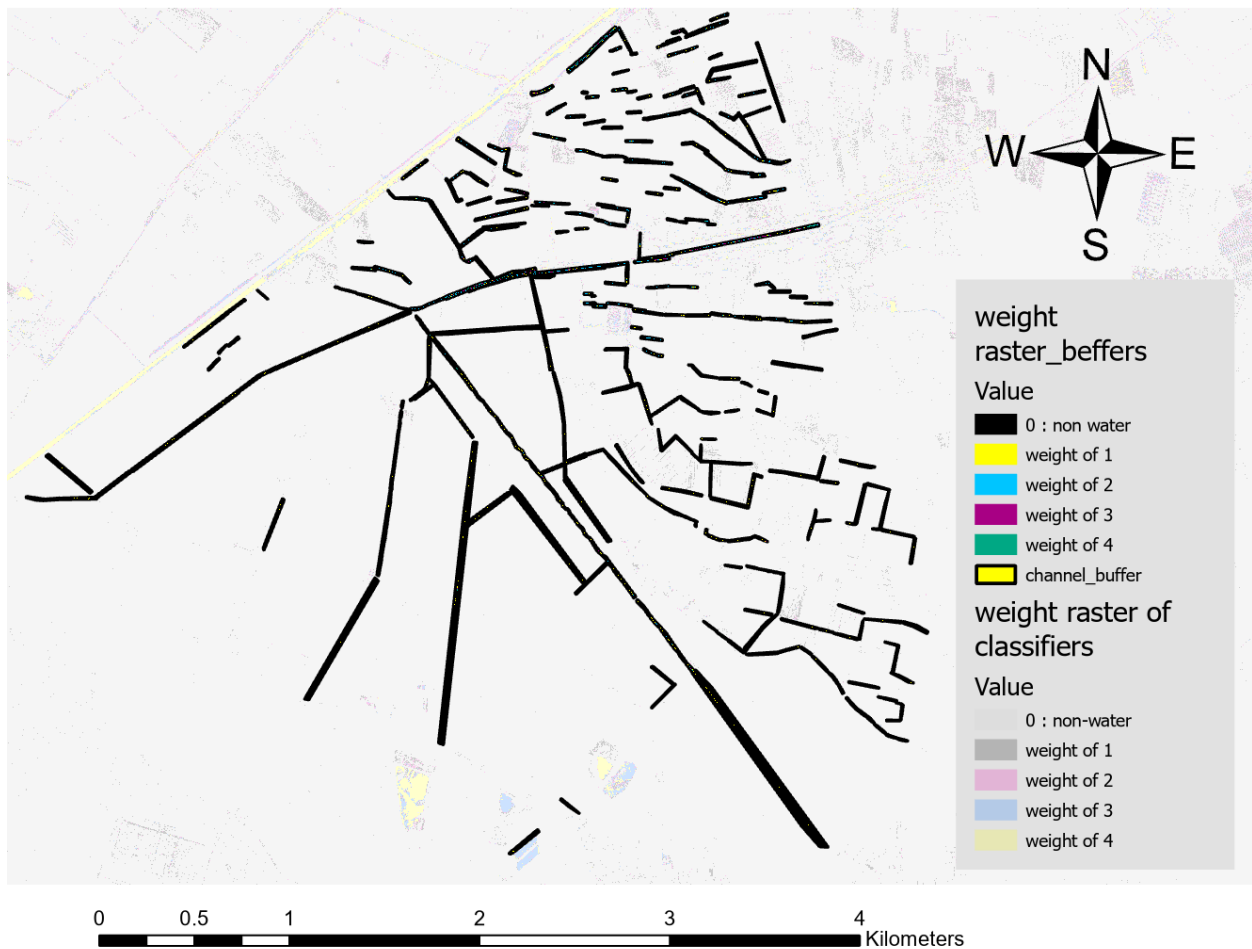


Figure 41- The weight raster masked for the buffers of the channels

Result

In the attribute table of each of those masked rasters, the number of pixels belonging to each value is calculated and is reported below.

| Value | Count |
|-------|---------|
| 0 | 2280593 |
| 1 | 54862 |
| 2 | 43534 |
| 3 | 15177 |
| 4 | 12775 |

Table 1- Number of detected water pixels related to each wight of 0 to 4

The attribute table of weight raster (table1) shows that the majority of pixels related to water channels are detected by 1 classifier (with 54682 pixels), or by 2 classifier (with 43534 pixels), while the lesser amount of those are belonging to weight of 3 or 4. (with respectively 15177 and 12775 pixels).

| Value | Count |
|-------|---------|
| 0 | 2317112 |
| 1 | 89829 |

Table 2- Number of detected water pixels by the SVM classifier

| Value | Count |
|-------|---------|
| 0 | 2325659 |
| 1 | 81282 |

Table 3- Number of detected water pixels by the random trees' classifier

| Value | Count |
|-------|---------|
| 0 | 2369481 |
| 1 | 37460 |

Table 4- Number of detected water pixels by the K-nn classifier

| Value | Count |
|-------|---------|
| 0 | 2376951 |
| 1 | 29990 |

Table 5- Number of detected water pixels by the maximum likelihood classifier

According to the above tables of the number of pixels of water channels detected by each classifier, the SVM and Random Trees classifiers made greater contribution in detection of fine lines of water with respectively 89,829 and 81,282 pixels detected, while effectiveness of K- nearest neighbor and Maximum Likelihood are significantly lesser than the other 2, with 37,460 and 29,990 pixels detected respectively.

3.2.5. Validation of classification result

Method

In order to ease the application of classification procedure to larger areas, simplified models that describe the results of classification are introduced, based on histogram analysis of every band. For each band regarding the distribution of the data, some ranges are introduced to filter the data. The model for detection of pixels of water channels is defined in a way that satisfies the range of filter for all the four bands. This step is performed using Python scripts.

In the below figure 41, the left-hand side rectangle in blue is the training zone of the models, and the right-hand side one in green is the test zone.

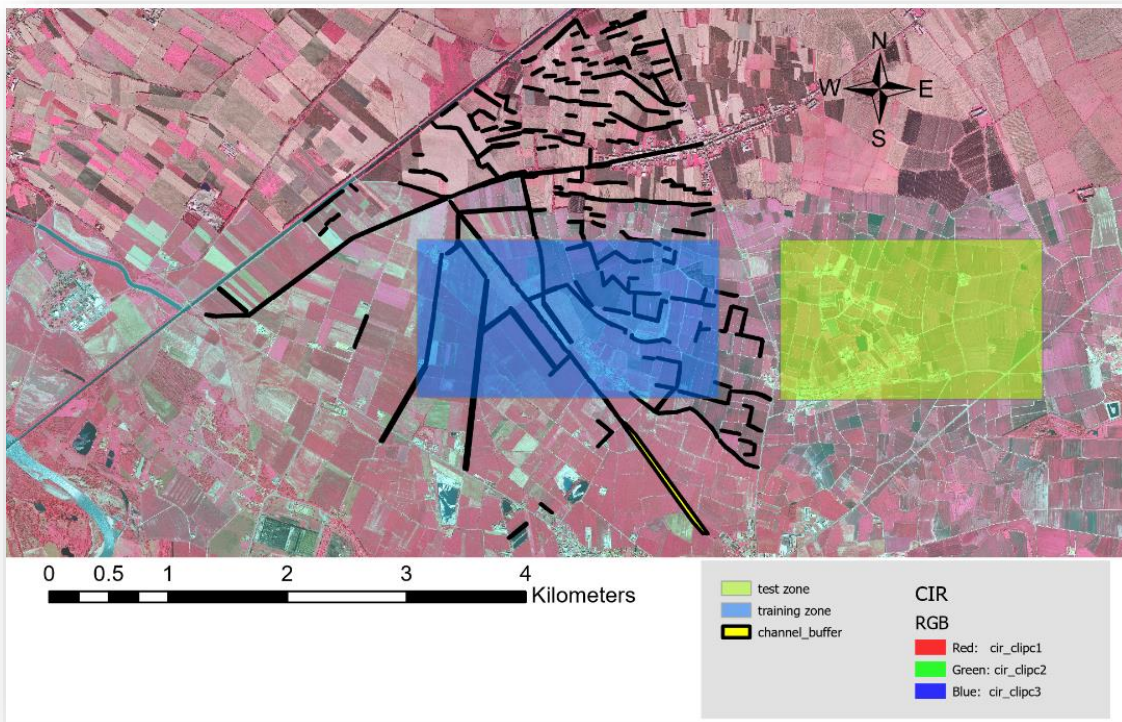


Figure 42- The training zone and the test zone for validation of the classification

Definition of two scenarios

To find the best model, 2 scenarios are compared. In the first scenario all of the water pixels detected in the classification step in the training zone are taken as the input data, while input data of the second scenario are only those water pixels detected in the classification step in the training zone that are located inside the channels buffers (buffer of channels reported in figure 33).

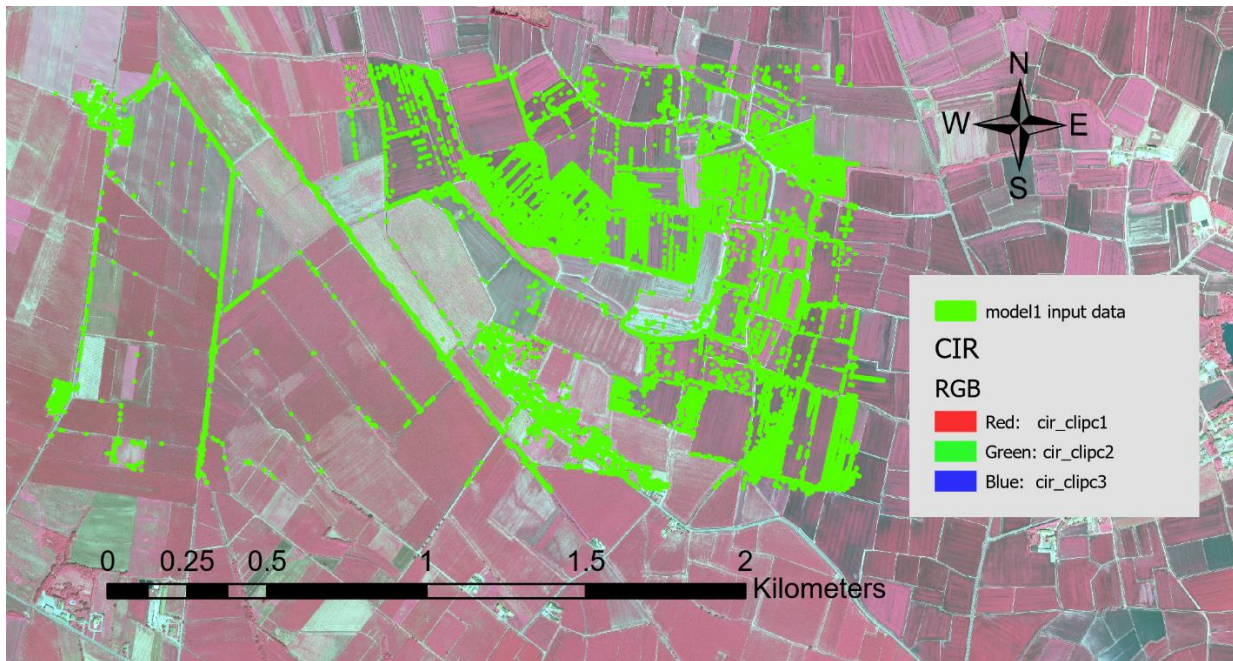


Figure 43- Input data of scenario 1 is only the water pixels resulted from classification which belong to the water channels

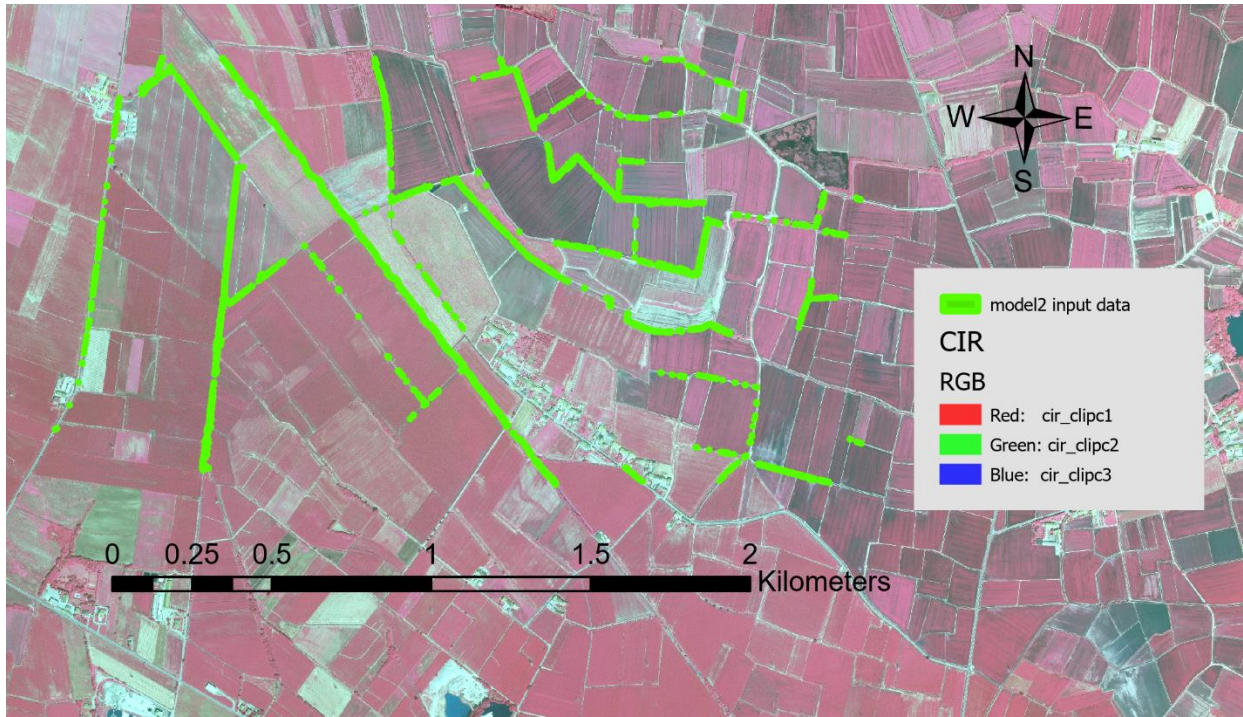


Figure 44- Input data of scenario 2 is all of the pixels detected as water in the classification step

The input data of scenario 1 reflects exactly the result of classification without any manipulation but is also affected by noises related to non-water pixels (roads and shadows), and some unwanted water pixels like water bodies and irrigation flooded fields. Input data of the second scenario, however, is refined to only pixels belonging to water channels and does not reflect the exact result of the classification step.

For each scenario the related water pixels are extracted and masked for the 4 bands of the images (RGB-NIR) and the histograms of each band are plotted, as well as histogram of the full subset of training.

Results

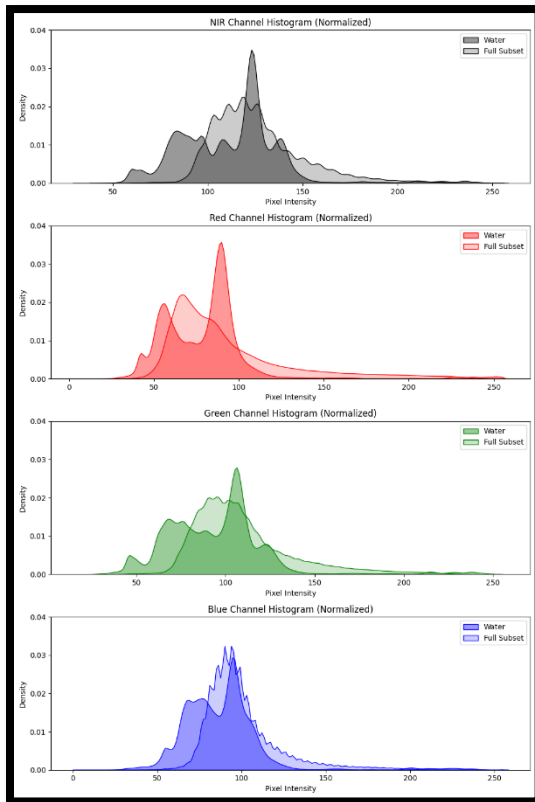


Figure 45- Scenario 1 : histogram of the water pixels versus the full subset , unit of pixel intensity : digital number

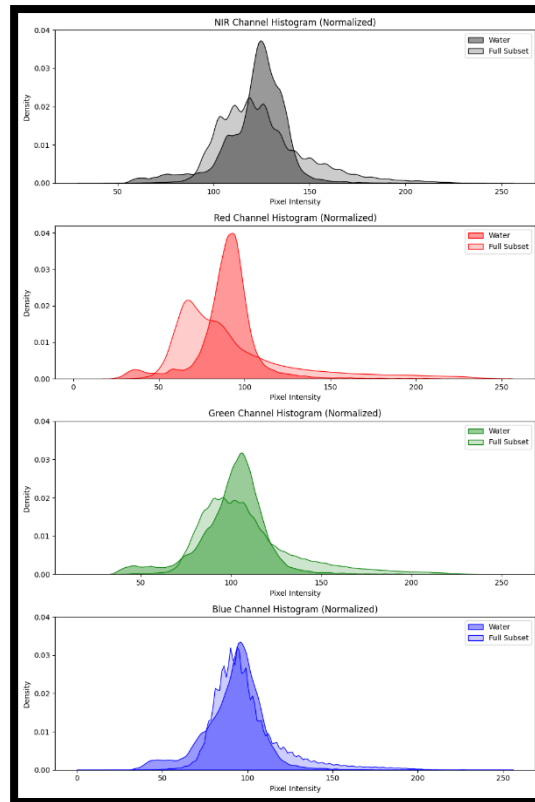


Figure 46- Scenario 2 : histogram of the water pixels versus the full subset , unit of pixel intensity : digital number

Extraction the range for filtering each band

Histograms of scenario 2 are fitted to a Gaussian distribution and mean and standard deviation of each band are calculated. Histograms of scenario 1, on the other hand, do not follow a Gaussian shape, and their distributions seem to be a combination of some distributions (gaussian mixture), with one peak being significantly higher than the others. For this reason, the highest peak is taken as the center of the range of presence of water, and only for the part of histogram that includes the highest peak, a gaussian distribution is fitted.

To find the best threshold for each histogram in scenario 1 and scenario 2, some different coefficients of the standard deviation of each gaussian distribution are applied on the train zone. For each coefficient that

results in a range on the histogram, the models are introduced in a way that satisfies the conditions for all of the four bands. It means that the model gives those pixels as the output result if values of all of those for bands are placed in the range introduced by the model. For each model with different coefficients of standard deviation, the area of truly detected pixels, and wrongly detected ones (as errors) is calculated.

The truly detected ones (True Positive) are those pixels resulted by the model, which is located inside buffers of the channels, and the wrongly detected ones (False positive) are those outside the buffers of the channels.

| Coefficient of the standard deviation for scenario 1 | Area of True Positive in square meter | Area of False Positive error in square meter |
|---|---------------------------------------|--|
| 0.2 | 16 | 769 |
| 0.4 | 160 | 7062 |
| 0.6 | 683 | 25928 |
| 0.8 | 1819 | 62617 |
| 1 | 3567 | 111222 |
| 1.2 | 7490 | 171038 |
| 1.4 | 11472 | 240385 |
| 1.6 | 17036 | 316753 |
| 1.8 | 25362 | 398751 |
| 2 | 49676 | 474451 |
| Classification | 5015 | 36537 |
| Model on the test zone | Area of the detected pixels : 54460 | |

Table 2- True positive and false positive values for each coefficient of standard deviation in the scenario 1

| Coefficient of the standard deviation for scenario 2 | Area of True Positive in square meter | Area of False Positive error in square meter |
|---|---------------------------------------|--|
| 0.2 | 580 | 11079 |
| 0.4 | 5638 | 107013 |
| 0.6 | 16347 | 290648 |
| 0.8 | 19383 | 483073 |
| 1 | 23898 | 675304 |
| Classification | 5015 | 36537 |
| Model on the test zone | Area of the detected pixels: 50565 | |

Table 3- True positive and false positive values for each coefficient of standard deviation in the scenario 2

For the scenario1 the model with coefficient of 1 is accepted, as it gives 3567 truly detected pixels which is the closest to the area detected as water by classification, however its False Positive error is large (111222 m²) comparing to the result of classification with 36537 m² of False positive error. For the second scenario, the standard deviation coefficient of 0.4 is accepted which results have the most similarity to the classification (5638 m² truly detected by the model, versus 5015 m² resulted from classification), similarly with large amount of commission error which is 107013 m².

| Scenario1 | Histogram | | Model 1 | |
|-----------|-----------|--------------------|---------------------------------|---------------|
| | Peak | Standard deviation | Width = 2*1* standard deviation | Center = Peak |
| Blue | 95.10 | 6.65 | 13.3 | 95.10 |
| Green | 105.18 | 7.80 | 15.6 | 105.18 |
| Red | 88.77 | 8.85 | 17.7 | 88.77 |
| NIR | 123.40 | 4.87 | 9.74 | 123.40 |

Table 4- Results of the scenario 1, unit: digital number

| Scenario 2 | Histogram | | Model 2 | |
|------------|-----------|--------------------|--------------------------------------|---------------|
| | Mean | Standard deviation | width = 2 * 0.4 * standard deviation | Center = mean |
| Blue | 92.07 | 19.07 | 15.25 | 92.07 |
| Green | 100.85 | 20.27 | 16.21 | 100.85 |
| Red | 89.75 | 19.35 | 15.48 | 89.75 |
| NIR | 121.53 | 18.17 | 14.53 | 121.53 |

Table 5- Results of scenario 2 , unit : digital number

Interpretation

Finally, comparing models 1 and 2, model 2 works better, as it results in lesser area of False positive error for the same area of truly detected pixels.

Both models are designed to detect fine lines of channels characterized by edging and mixed water pixels, rather than pure water pixels. As such, they do not detect pure water bodies, like lakes or wide channels, but instead focus on the edging pixels of wider water channels, without capturing the main body of these channels.

To detect all water pixels in an image, traditional water detection indices are also useful. Therefore, a combination of the model introduced in this study and standard water detection methods can effectively cover all water bodies and channels, from narrow to wide.

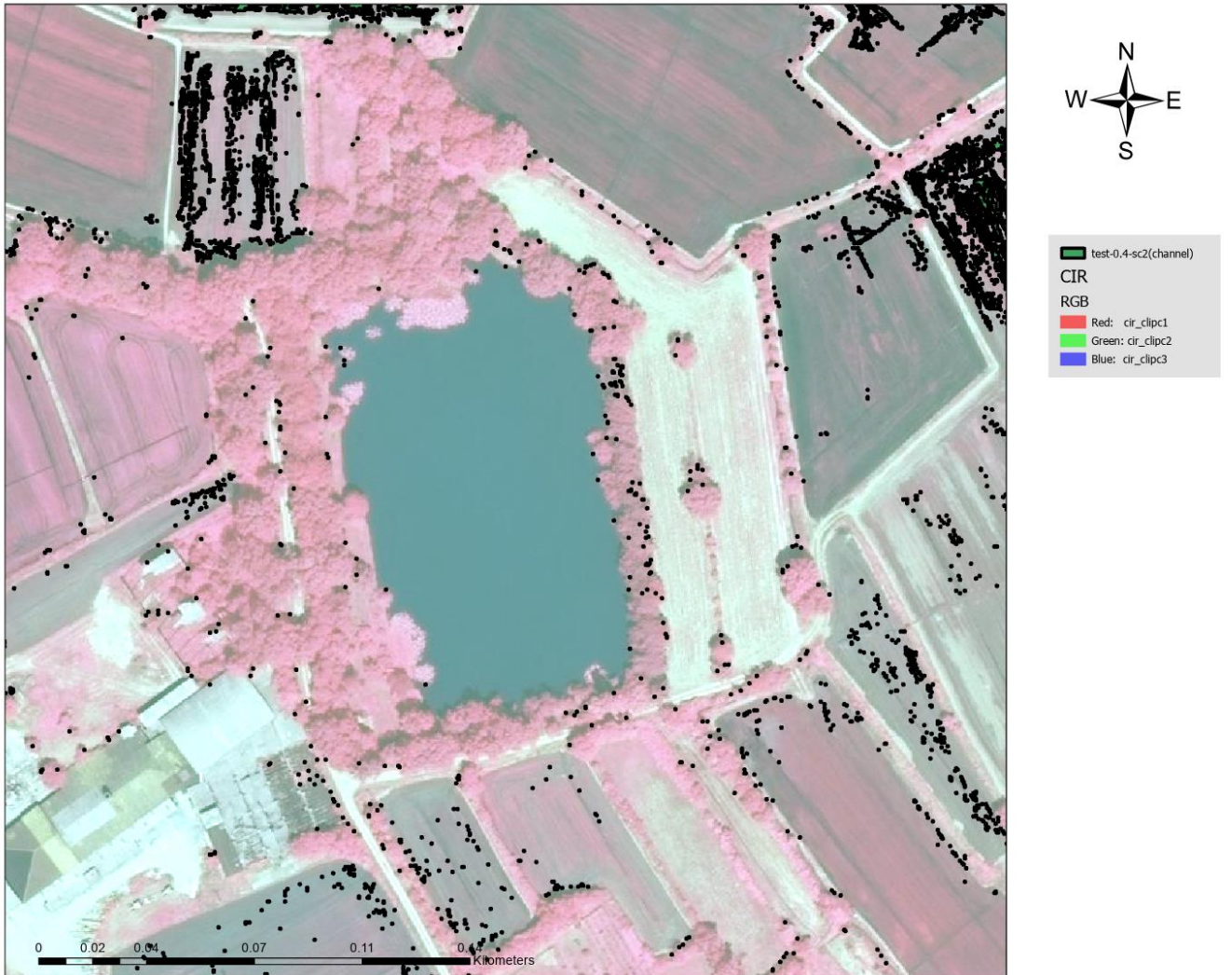


Figure 47- The model does not serve for detection of major water bodies such as lakes



Figure 48- Application of the model to the test zone

3.2.6. Extraction of channel polygons

Method and results

In this step, the complete polygons representing the channels are created by connecting the scattered water polygons resulting from the classification step which is reported in figure 32 . Figure below (48) shows an example of scattered polygons representing a segment of a channel.



Figure 49- The scattered polygons detected as water channel

In order to generate a continuous polygon for each channel segment, the water polygons are first converted to points, located on their central locations. Next, lines are generated by connecting the points that belong to the same channel segment. Along these lines, rectangles with predefined dimensions are created. These rectangles are then dissolved into a single feature. For a better visual appearance, the polygons are smoothed, and any voids within them are eliminated. This process is carried out using the following sequence of tools:

- Feature to Point :

Creates a feature class containing points generated from the centroids of the input features or placed within the input features. The input feature class of this step is the water polygons extracted from the classification step.

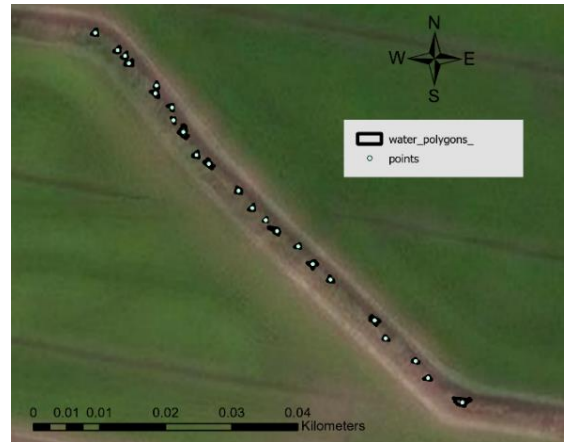


Figure 50- Polygons converted to points located at their centroid

- Points to Line :

Generates lines that connect the points which were created in the previous step.



Figure 51- Lines are generated from the points

- Generate Rectangles Along Lines :

Creates a series of rectangular polygons that follow a single linear feature or a group of linear features.



Figure 52- Rectangles are generated along the lines

- Dissolve Boundaries :

This task simplifies the geographic datasets by merging adjacent or overlapping polygons that share common attributes.



Figure 53- The rectangles are dissolved

- Smooth Polygons :

Smooths sharp angles in polygon outlines to improve aesthetic or cartographic quality.

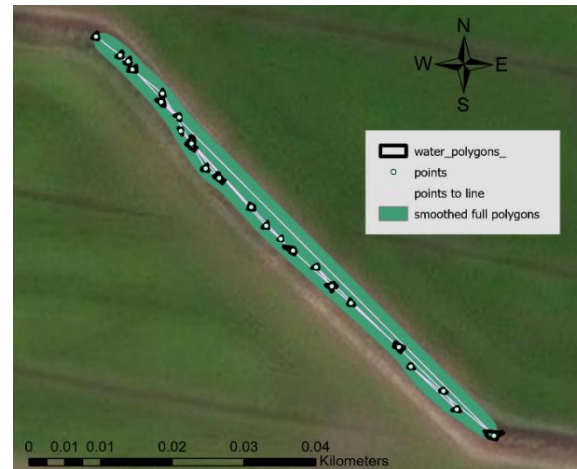


Figure 54- The dissolved rectangles are smoothed

- Eliminate Polygon Part :

Creates a new output feature class containing the features from the input polygons with some parts or holes of a specified size deleted.

Model Builder

To streamline and speed up the process, this sequence of tools can be combined into a single model using the Model Builder tool, allowing for all steps to be executed with one click. ESRI's ModelBuilder, is an ArcGIS application to create, edit, and manage models. In ModelBuilder, the model is represented by a flux diagram in a graphic user interface which facilitates to create, visualize, edit, and execute geoprocessing workflows, to use and reuse them, to share and apply them to different geographic areas.

Advantages of using ModelBuilder

- Time Efficiency: By automating the workflow, ModelBuilder saves significant time, as all steps can be executed with a single click rather than running each tool individually.
- Optimized Data Management: ModelBuilder allows for saving only the result of the final step, reducing the need to store intermediate data and thus saving storage space.
- Reproducibility: The model can be easily reused with new input data, allowing the procedure to be repeated consistently for similar tasks or different datasets[30].

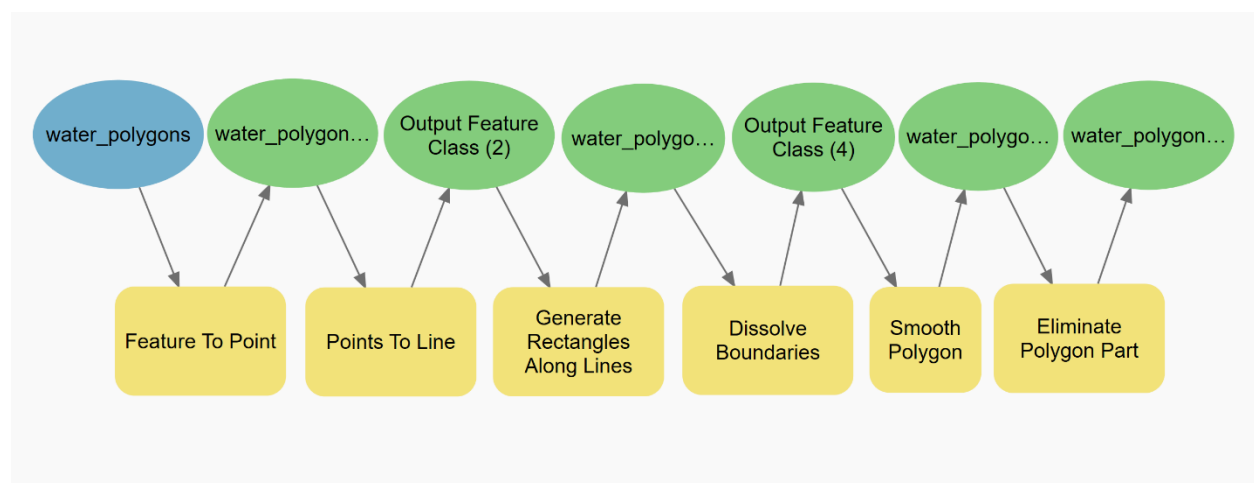


Figure 55- Model builder to generate polygons of channels from the scattered water polygons

Propagation of the model over the entire area using iteration

Once each buffer is intersected with the entire image of water polygons, the polygons inside that buffer can be selected and processed through the model to create the channel geometry. A new model is built using ModelBuilder with iteration that can automate this task. (Figure 55).

Using the iteration component in the model, the process of intersecting the channel buffer with the water polygons is performed sequentially for each buffer polygon, using the ID field as a counter. At the final

stage of the model, the results of each iteration are collected using the "Collect Values" tool, a specific function of ModelBuilder. Finally, the "Merge" tool is used to combine the output from each iteration, creating a complete feature class of the channel polygons.

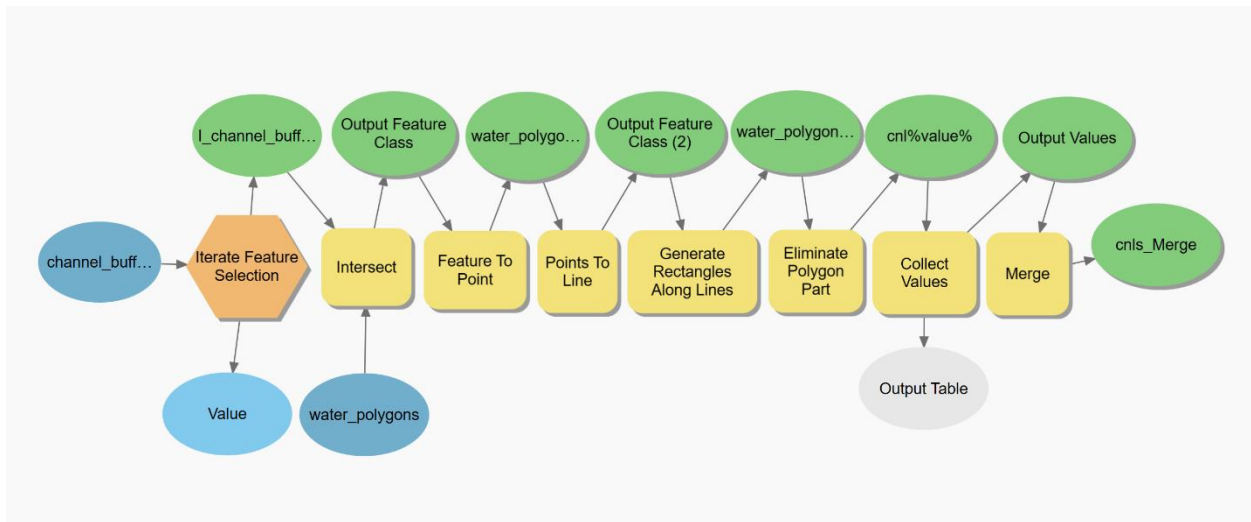


Figure 56- Model Builder with iteration to propagate the generation of the channels polygons to the entire subset

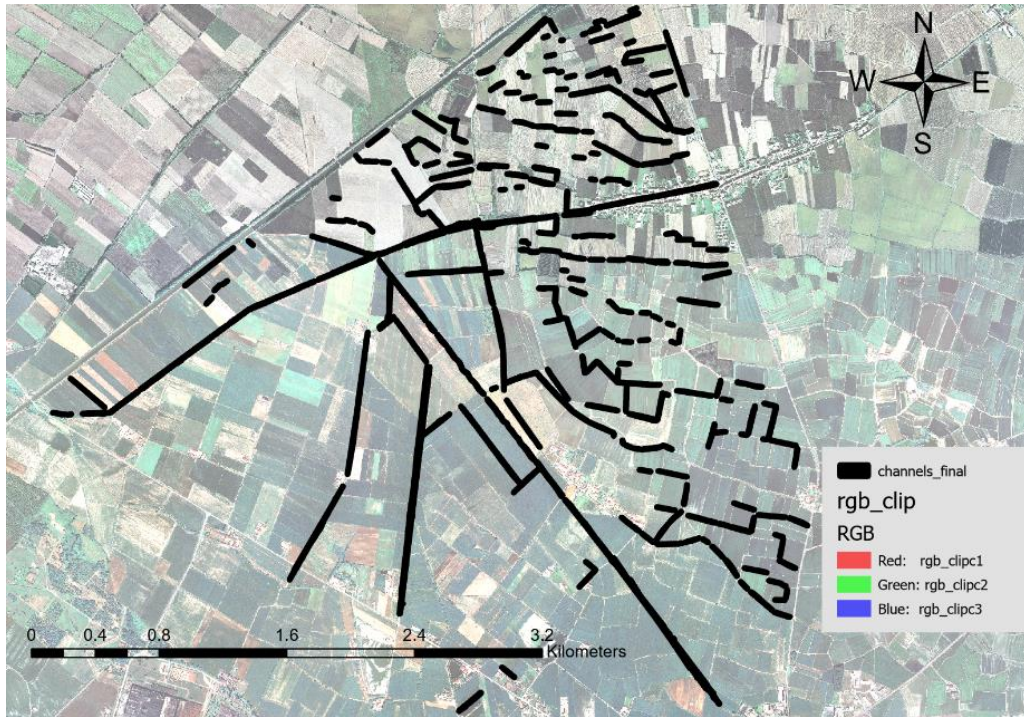


Figure 57- Final result of the model, every piece of channel is generated

3.2.7. Accuracy assessment

Deficiencies/Issues with the result

One potential issue that may introduce errors when running the model occurs if a channel buffer covers only a single water polygon. In this case, the model converts the polygon into a single point, making it impossible to generate a line from just one point. This issue can be resolved by splitting that water polygon into smaller segments. With multiple polygons converted into points, lines can then be created, allowing the subsequent steps to be carried out as expected.

Another issue arises when a large water polygon located at the endpoint of a channel is converted into a point, and the model subsequently generates a new polygon from that point along with others. In this case, a substantial portion of the channel may be omitted. Additionally, the resulting polygons may include areas that do not, in reality, belong to the water channel.

To assess the model's accuracy, two types of errors are introduced: commission and omission errors.

- **Commission errors** are areas incorrectly mapped as water but are not water in reality.
- **Omission errors** are areas that represent part of the water channel but are not captured by the model.

To evaluate the extent of these errors, the real geometry of the channels is created for two sample areas based on the orthophotos, which can be considered as ground truth data. The area of commission error is identified by subtracting the accurate ground truth data from the model-generated channel geometry, while omission error is determined by subtracting the model-generated geometry from the accurate ground data.

Sample 1

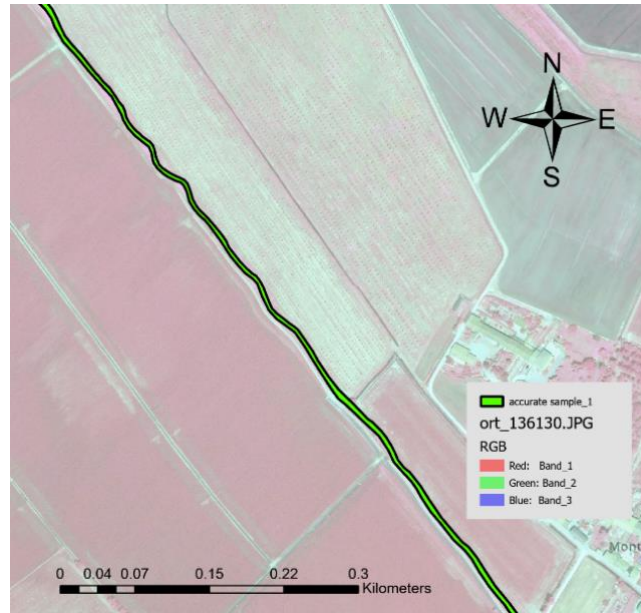


Figure 58- The accurate sample1

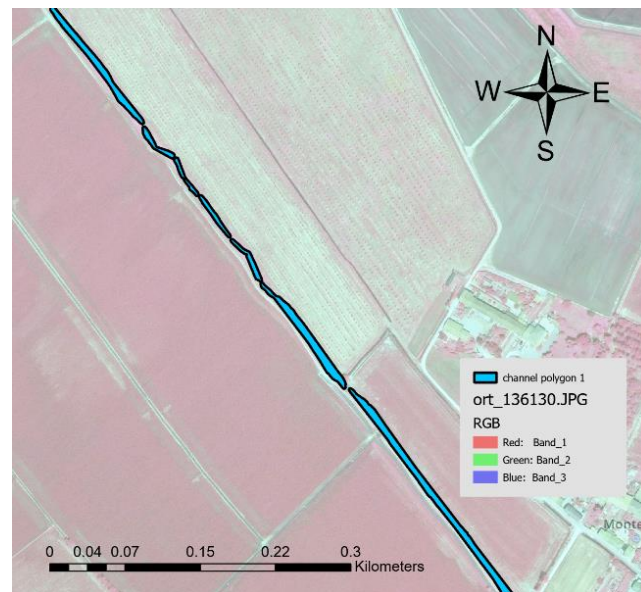


Figure 59- Channel polygons generated by the model, sample1

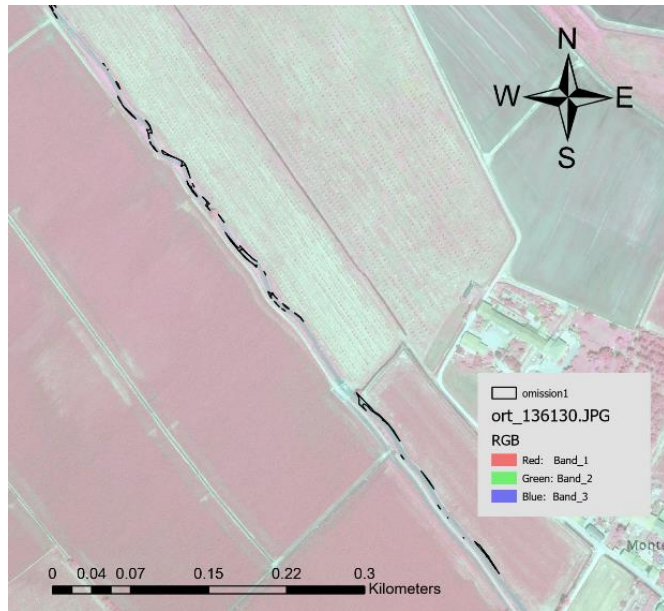


Figure 60- The omission error of sample 1

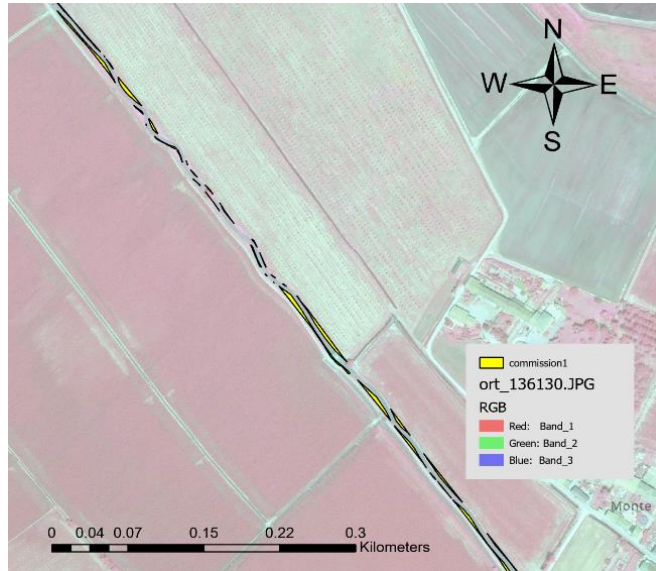


Figure 61- The commission error of sample 1

Sample2

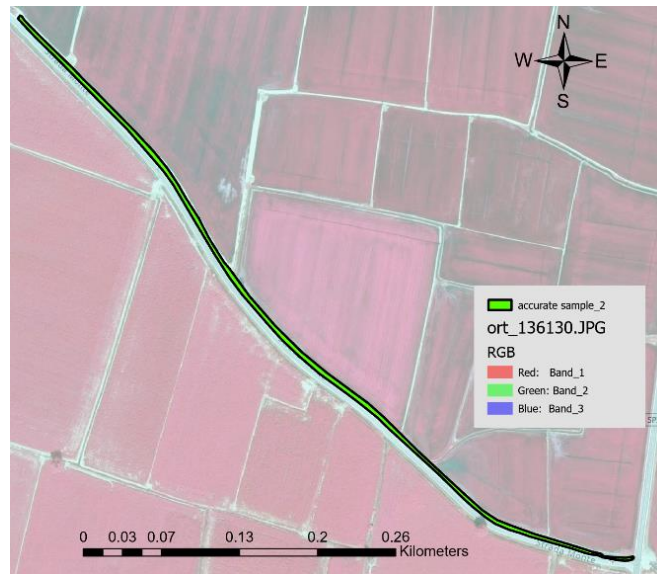


Figure 62- The accurate sample2

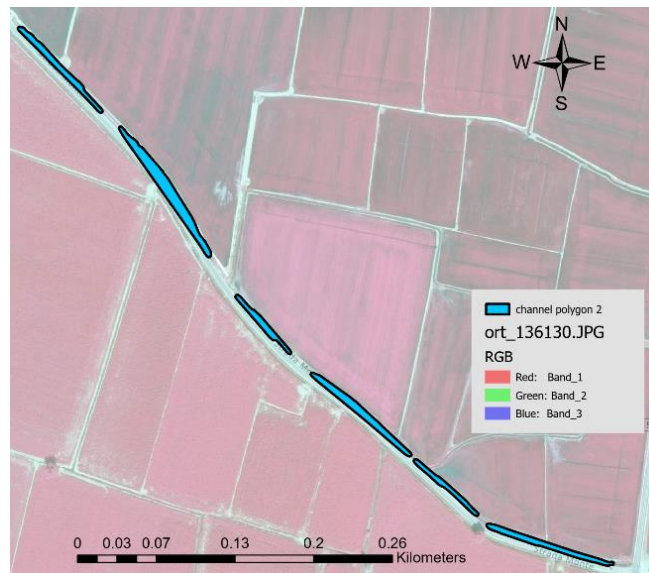


Figure 63- Channel polygons generated by the model, sample 2

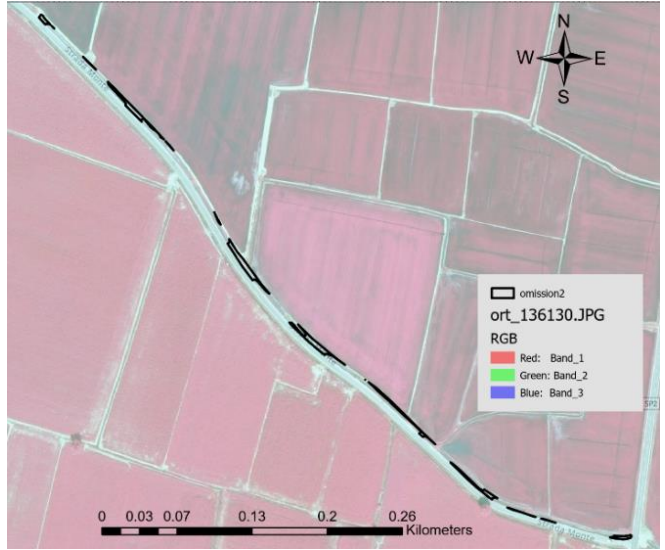


Figure 64- The omission error of sample 2

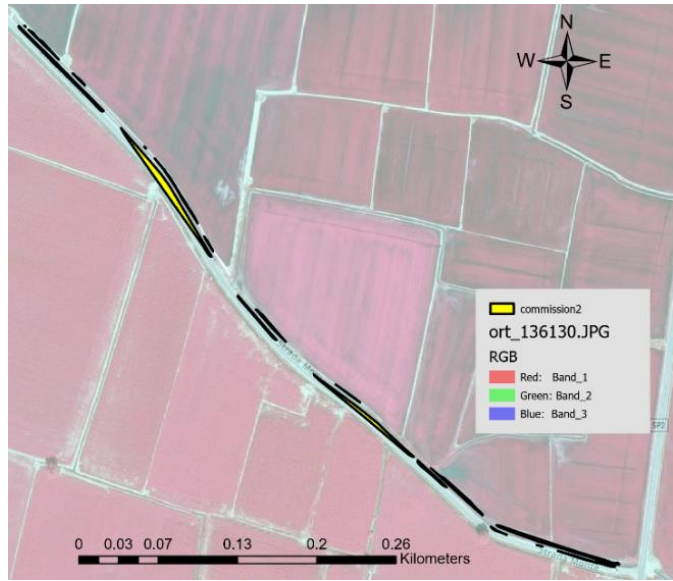


Figure 65- The commission error of sample 2

Results

Area of commission and omission errors are calculated and presented in the table below, along with the percentage of each error, which is determined by dividing each error by the area of the accurate ground truth data. (Table 10)

| sample | area of accurate sample | area of model result | area of omission error | area of commission error |
|--------|-------------------------|----------------------|------------------------|--------------------------|
| 1 | 7805 | 10233 | 1087 | 3515 |
| 2 | 2463 | 3057 | 654 | 1248 |

| omission error / Accurate sample | commission error / Accurate sample |
|----------------------------------|------------------------------------|
| 0.14 | 0.45 |
| 0.26 | 0.5 |

Table 6- Accuracy assessment of the model to generate polygons of the channels

unit of area: square meter

According to table 10, the percentage of commission error appears significant. This could be attributed to both the predefined width of the channel and instances where vegetation obscures the channels.

3.2.8. Determining the flow direction in channels

The data used for this objective includes the line feature of the channels and a DTM (Digital Terrain Model) of the area, with a 5-meter pixel size and 1-meter resolution in elevation. Since the study area overlaps with two images, the images are mosaiced and clipped to match the study area.

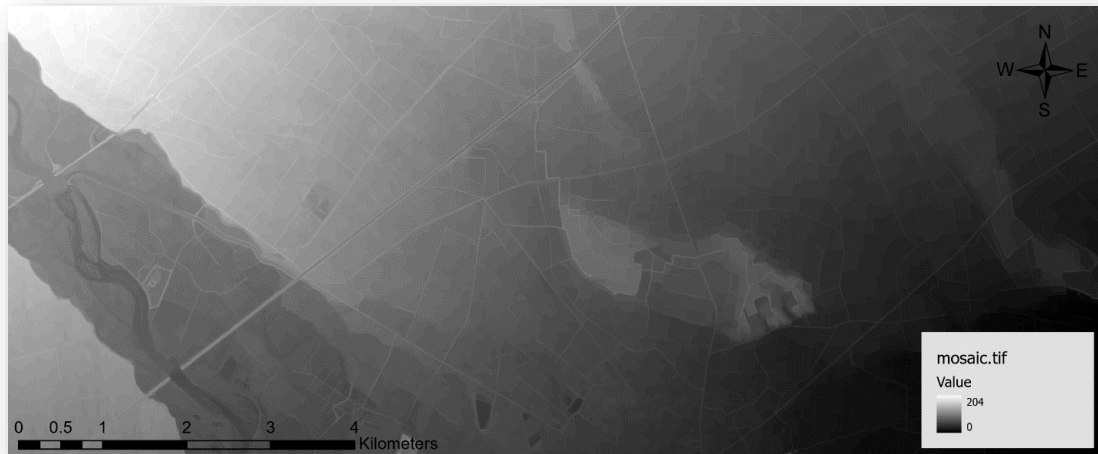


Figure 66- The Digital Elevation Model with 5 meters pixel size and 1 meter resolution in elevation, the values of elevation are reported in meter, from 0 to 204 m

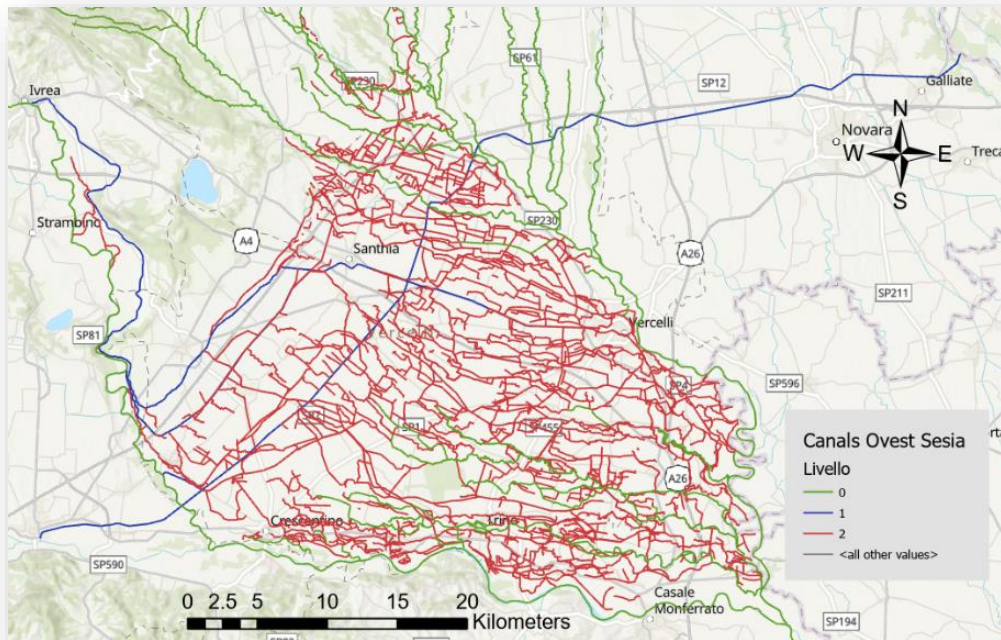


Figure 67- The line features of the channels, with 3 levels, where level 0 represents natural streams and rivers, level 1 represents the main channels like Cavour, and level 2 represents the principal irrigation channels

First, a collection of point features is created (figure 67), representing the endpoints of each line or key vertices along the channel lines. Using the "Extract Value to Point" tool, to each point the DTM value is assigned from the pixel on which the point is located, that represents the elevation of that point. At this stage, it is assumed that the channel bed elevation is equal to the ground elevation.

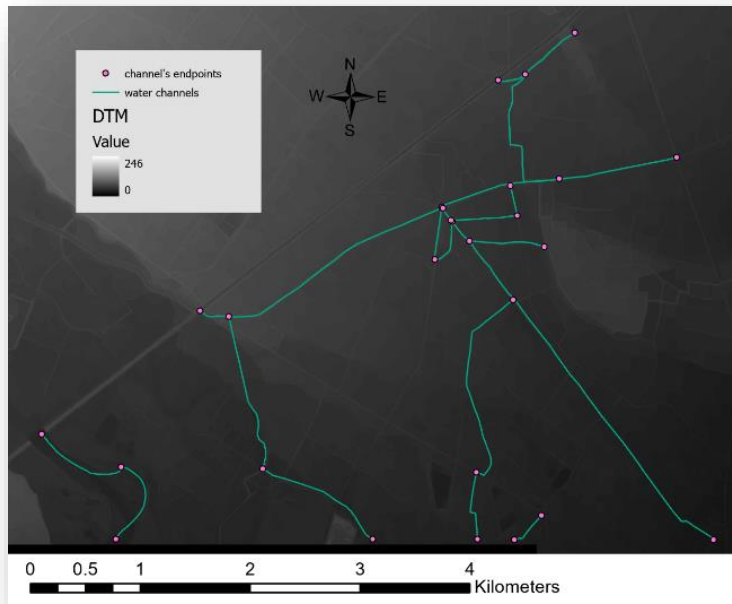


Figure 68- The end points of the channels

Next, a line with symbology of arrows is created to connect two of these points. By assigning direction to the line based on the elevation values of the points, the arrow direction goes from the lower elevation to the higher one. However, since water flows from higher to lower elevation, the elevation values are negated using the "Calculate Field" tool. With the negative elevation values, as the sort field of points, the generated arrowed line between the two points will be directed from the higher elevation to the lower one, correctly indicating the flow direction. (figure68)



Figure 69- Direction of flow determined by arrows between 2 points

Model Builder for flow direction

To automate this process, a new Model Builder tool is created. The model takes the point features, converts them into a line, and assigns the arrowed line as its symbology.

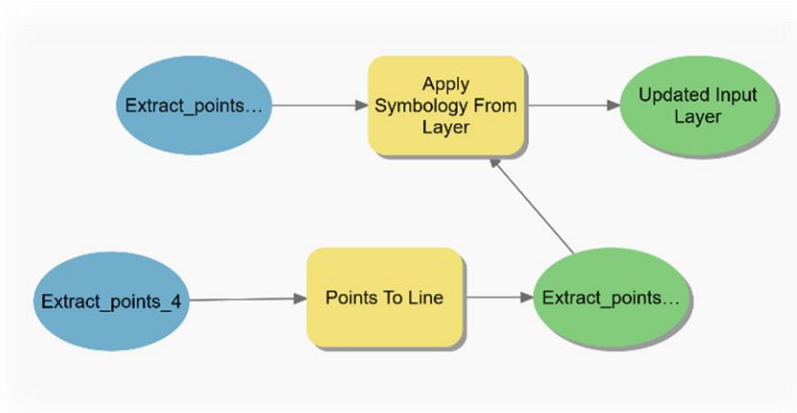


Figure 70- Model builder to generate arrowed line between 2 points which determines the direction of flow

Before running the model, it is essential to select only the two endpoints of a channel. The model then executes based on these selected points.

It's important to note that the model works effectively only when the two points are far apart enough to exhibit an elevation difference of more than one meter. If the points are too close and their DTM-based elevation values are similar, the derived flow direction will be inaccurate or misleading.

4. Discussion

4.1. Improvement of channel documentation and flow direction detection

The results of this study highlight the improvement in documenting water channels, revealing previously recorded segments and also unrecorded ones that were not reflected in existing line features, with time spent as reported in the table below (11). This enhancement broadens our understanding of the current network of channels, though some polygons generated were imperfectly integrated and showed minor errors. Despite these limitations, these polygons provide valuable insights into the locations and directional flow patterns of the channels. Using Digital Terrain Model (DTM) data could further clarify flow direction within these channels, although a higher-resolution elevation dataset would be advantageous. In cases where elevation differences between channel endpoints are minimal (often around 0.2 to 0.3 meters) such precision is challenging to capture with the 1-meter resolution elevation data used in this study.

The polygonal representation of channels offers another benefit: the potential to detect water presence and assess both water quality and quantity within these channels. To achieve this, data from satellite or airborne imagery with suitable spatial resolution is essential.



Figure 71- The model could successfully detect the existing recorded channels and many unrecorded ones

Table of timing

| Step | Details | Time Spent |
|---|--|-------------------|
| Data | Download and preparation of the data | 1 hour |
| CIR image classification | Generating the training samples | 1 hour |
| | Running of the 4 classifiers, extracting water from each, and aggregation | 1 hour |
| RGB image classification | Generating the training samples | 1 hour |
| | Running of the 4 classifiers, extracting water from each, and aggregation | 1 hour |
| Channels buffer | Manual creation of buffer of channels for the whole subset | 10 hours |
| Evaluation of performance of each classifier | Generating the binary rasters , the weight raster, and extracting them all for the mask of buffers | 1 hour |
| Validation of classification step | Exporting data from Arcgis to Python, preparing the datasets of each scenario and generating the histograms | 3 hours |
| | Fitting the histograms to specific distributions, applying different ranges, and exporting the results in shapefile format | 4 hours |
| | Calculating area of false positive and true positive for each range | 3 hours |
| Generating polygons of the channels | Exploring method for generating polygons of channels from the scattered pixels | 1 hour |
| | Generating the model builder | 10 minutes |
| | Run the model builder for the entire subset | 5 hours |
| Accuracy assessment | Drawing accurate samples, and extracting areas of commission and omission error | 2 hours |
| Direction of flow | Exploring method for determining the direction of flow | 1 hour |

Table 7- Time consumed on each step of the work

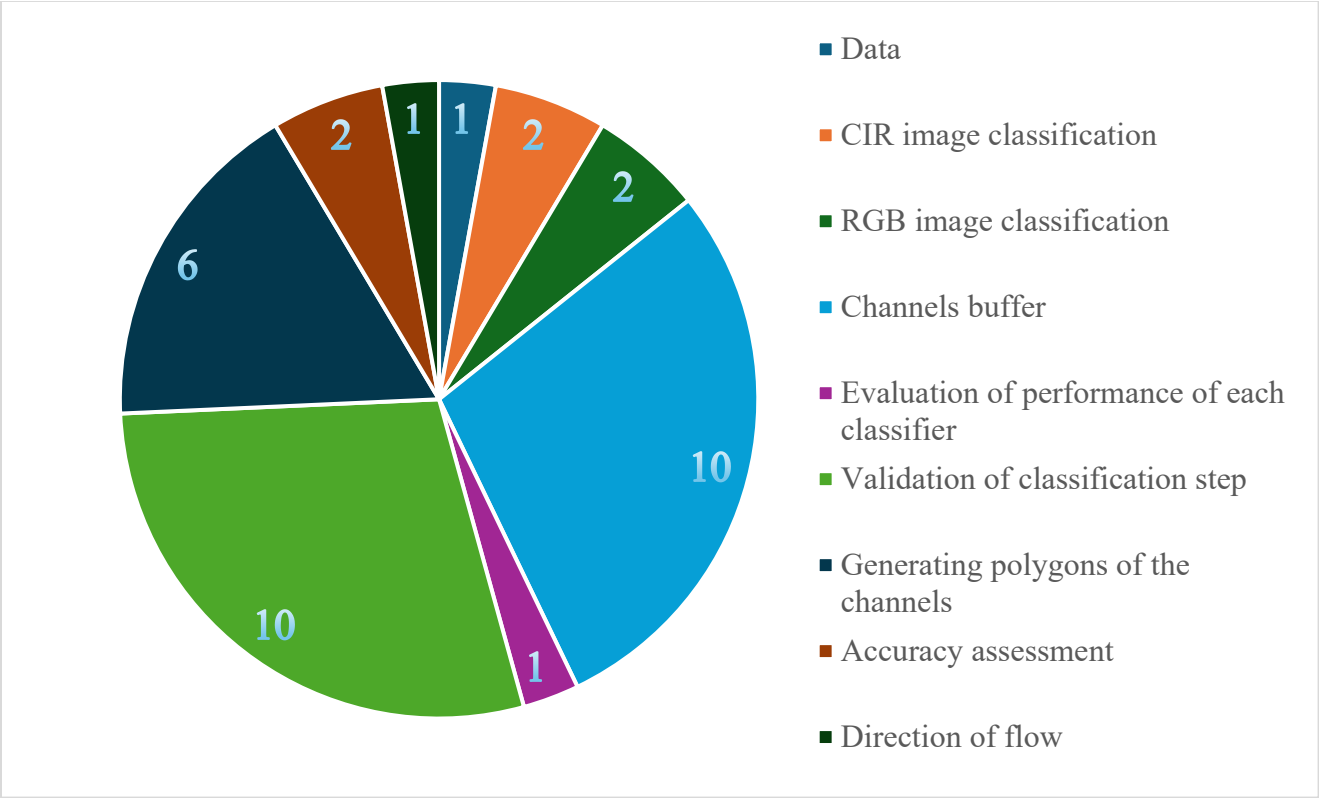


Figure 72- Bar chart of time consumed for eacg step of the work

4.2. Multi temporal analysis using channel geometry and Sentinel-2 data

The final channel polygons can serve as reference geometries for temporal analysis to observe water presence in the channels over time or detect changes by overlapping these polygons with high-resolution satellite imagery. In this study, Sentinel-2 images were used to assess temporal variations. By using images taken at different times of the year (for instance, during summer when irrigation channels are typically full, and winter when they are often dry) this analysis aimed to detect changes in presence of water in the channels. Each image overlap was analyzed using the Modified Normalized Difference Water Index (MNDWI), which uses the green and shortwave infrared (SWIR) bands. However, the results did not produce values that indicated water presence.

Conversely, the Normalized Difference Vegetation Index (NDVI), based on the difference between red and near-infrared (NIR) bands, did reveal vegetation within the polygons. This finding suggests that for a Sentinel-2 pixel resolution of 10x10 meters, covering a channel width of approximately 2-4 meters, the pixel's reflectance likely captures vegetation presence rather than water. Sentinel-2's 10-meter resolution is therefore insufficient for precise channel water detection in this context. Higher-resolution imagery, such as that from GeoEye, WorldView-3, or Planet's SkySat, with pixel size of around one meter or less, may provide the necessary spatial detail for effective temporal analysis. Alternatively, drone-based multispectral imagery, offering resolutions down to a few centimeters, could be particularly valuable for mapping channel geometry with high accuracy, and multi temporal analysis.

4.3. Classification challenges and spectral coverage limitations

During the classification process, certain channel segments were visible but remained undetected by classifiers, likely due to limited spectral coverage, as only four bands were used in this study. Higher spectral resolution within existing bands and additional bands at longer wavelengths, such as SWIR, could improve water pixel differentiation. SWIR data is also beneficial for detecting shadows and built areas, which would further aid in distinguishing water bodies more accurately.

4.4. Necessity of repetition of the acquisition

Water remains in each area of irrigation for approximately 2 to 3 weeks before being directed to lower-elevation areas. In the study area, channels in the upper section were fully watered, while those in the lower left section appeared empty, with fields also showing dryness in these areas. To effectively monitor the entire irrigation network, data acquisition at least every two weeks would be ideal. Sentinel-2's 5-day revisit rate provides sufficient temporal resolution for this purpose and offers good spectral coverage, particularly in the near-infrared range, allowing for the calculation of water indices. However, comparison with ground truth data revealed that channels were often undetectable in Sentinel-2 images due to their 10-meter spatial resolution, insufficient for channels averaging 2 to 4 meters in width.

For this reason, orthophotos from the Regione Piemonte cartographic sector were used as an alternative. These orthophotos offered greater spatial resolution but lacked the spectral resolution and coverage of Sentinel-2 data. Moreover, the orthophotos were limited to a single acquisition date, restricting temporal analysis. If channel polygons could be extracted from multiple image acquisitions, it would be possible to merge them into a more complete representation of the irrigation network.

4.5. Classifier selection and performance

Among the classifiers evaluated, Support Vector Machine (SVM) and Random Forest demonstrated the highest effectiveness in detecting water channels, showing significant contributions in the classification process. Therefore, for similar future analyses, this study recommends using Random Forest or SVM classifiers, or a combination of both, to enhance the accuracy of channel detection.

4.6. An open challenge

Another significant challenge in detecting water channels within the study area was the frequent obstruction of channels by overhanging tree branches. In many cases, these branches blocked the channels from view, rendering them partially or entirely invisible in the imagery. This obstruction is a substantial and largely unsolvable issue, as the vegetation obscures the spectral and visual signatures of the water channels beneath. These visual impediments reduce the accuracy of channel mapping and detection, as spectral data cannot penetrate dense canopy cover effectively.



Figure 73- The CIR image



Figure 74- Imagery base map of ArcGIS pro

The right-hand side image above (figure 72), is an irrigation channel from imagery basemap of ArcGIS pro, the left-hand side one (figure71) is the same area from the CIR image which is source of this study. While in the right-hand side image, a wide channel is visible, in the left hand side one, it is almost fully covered by branches of nearby trees.

5. Conclusion

This research introduces methods for mapping and analyzing the irrigation networks, focusing on the case study of Cavour Channel in Piemonte, Italy, by using aerial multispectral data. This study addresses the criticalities of mapping narrow and complex irrigation grid of channels, with the purpose of sustainable water management and climate resilience.

The use of four supervised pixel-based classification algorithms (K-Nearest Neighbor, Random Trees, Support Vector Machine, and Maximum Likelihood) allowed for a comparative assessment to determine the most effective algorithm for identifying narrow water bodies which results in mostly edging and mixing pixels. The outcomes highlighted the strengths of Support Vector Machine and Random Trees in detecting fine water channels, while the K-Nearest Neighbor and Maximum Likelihood algorithms proved to be less effective. Aggregating the classification outputs from all four algorithms allowed for the creation of robust, inclusive water polygons that could reliably represent the channels in the study area.

The study developed models based on the histograms of each spectral band, which serve as simplified methods to validate the classification results. This validation process provides confidence in the capability of generalization of the approach to other regions with similar irrigation systems.

From the scattered detected water pixels, the complete channel polygons are generated using the tools of ArcGIS pro, to ensure the spatial coherence of geometry of channels as a usable map features. Buffer zones around each channel were created to ensure that polygons accurately reflected the channel segments while excluding misclassified pixels, such as shadows or roads. To further refine the channel mapping process, an iterative model was developed using ArcGIS Pro, which allowed for the automatic application of the model over the entire area of study.

The Digital Terrain Model (DTM) data combined with ArcGIS Pro tools is employed to determine flow directions in the channels. Based on elevation difference between the two endpoints of the channels, the direction of water flow within the irrigation network, is visualized, a critical aspect for understanding water distribution and optimizing irrigation efficiency.

Additionally, this research addressed practical challenges in water mapping, such as spectral variations in water due to turbidity, surface foam, and shadow. The combination of RGB and NIR bands was essential in distinguishing water from vegetation, soil, and built-up areas, achieving high classification accuracy despite the absence of Short-Wave Infrared (SWIR) bands, which are typically useful in water detection. The

findings emphasize the importance of using both visible and near-infrared wavelengths in areas with complex agricultural landscapes.

From a broader perspective, this research aligns with global goals to improve water use efficiency and supports climate-smart agriculture by providing a replicable methodology for mapping and managing irrigation systems. Automated mapping of irrigation networks not only enhances water management practices but also aids in responding to the growing water demands caused by climate change. This approach supports the sustainable use of water resources in agriculture, which consumes a significant portion of global freshwater and is increasingly challenged by changing weather patterns and limited water availability.

Future research could explore integrating this methodology with sub-metric pixel size satellite data to monitor water presence dynamically, enabling management in response to seasonal changes and water scarcity. Also acquisition or access to better band coverage and spectral resolution may solve the challenges faced in this study. Moreover, improved spatial mapping of polygons with better integrity or using real width of each section of channels may improve the accuracy of results in an effective way.

In conclusion, this study demonstrates the effectiveness of automated, multispectral data-based methods for mapping and managing irrigation networks. The research not only advances the technical tools available for water resource management but also offers practical insights into preserving vital water systems under shifting climate conditions, providing a model that could benefit other agricultural regions around the world.

Bibliography

- [1] “<https://www.italia.it/en/piedmont/il-canale-cavour>.”
- [2] “Atlas of Italian Irrigation systems.”
- [3] “<https://www.ovestsesia.it/cosa-facciamo/gestione-rete-irrigua/>.”
- [4] “<https://www.parcopiemontese.it/pun-dettaglio.php?id=970>.”
- [5] D. Tilman and M. Clark, “Food, Agriculture & the Environment: Can We Feed the World & Save the Earth?,” *Daedalus*, vol. 144, no. 4, pp. 8–23, Sep. 2015, doi: 10.1162/DAED_a_00350.
- [6] D. D. Zhang *et al.*, “The causality analysis of climate change and large-scale human crisis,” *Proceedings of the National Academy of Sciences*, vol. 108, no. 42, pp. 17296–17301, Oct. 2011, doi: 10.1073/pnas.1104268108.
- [7] A. K. Chapagain and A. Y. Hoekstra, “The blue, green and grey water footprint of rice from production and consumption perspectives,” *Ecological Economics*, vol. 70, no. 4, pp. 749–758, Feb. 2011, doi: 10.1016/j.ecolecon.2010.11.012.
- [8] H. C. J. Godfray *et al.*, “Food Security: The Challenge of Feeding 9 Billion People,” *Science (1979)*, vol. 327, no. 5967, pp. 812–818, Feb. 2010, doi: 10.1126/science.1185383.
- [9] J. A. Rodríguez Díaz, E. K. Weatherhead, J. W. Knox, and E. Camacho, “Climate change impacts on irrigation water requirements in the Guadalquivir river basin in Spain,” *Reg Environ Change*, vol. 7, no. 3, pp. 149–159, Aug. 2007, doi: 10.1007/s10113-007-0035-3.
- [10] A. Moragues-Faus, “How is agriculture reproduced? Unfolding farmers’ interdependencies in small-scale Mediterranean olive oil production,” *J Rural Stud*, vol. 34, pp. 139–151, Apr. 2014, doi: 10.1016/j.jrurstud.2014.01.009.
- [11] G. Fontanelli *et al.*, *Mappatura della coltivazione e monitoraggio della crescita di riso nel distretto agricolo di Salonicco (Grecia) tramite l’utilizzo di dati SAR*. 2015.

- [12] N. S. Diffenbaugh and F. Giorgi, “Climate change hotspots in the CMIP5 global climate model ensemble,” *Clim Change*, vol. 114, no. 3–4, pp. 813–822, Oct. 2012, doi: 10.1007/s10584-012-0570-x.
- [13] J. Schilling, K. P. Freier, E. Hertig, and J. Scheffran, “Climate change, vulnerability and adaptation in North Africa with focus on Morocco,” *Agric Ecosyst Environ*, vol. 156, pp. 12–26, Aug. 2012, doi: 10.1016/j.agee.2012.04.021.
- [14] W. W. Immerzeel *et al.*, “Importance and vulnerability of the world’s water towers,” *Nature*, vol. 577, no. 7790, pp. 364–369, Jan. 2020, doi: 10.1038/s41586-019-1822-y.
- [15] F. van Steenberg, A. M. Haile, T. Alemehayu, T. Alamirew, and Y. Geleta, “Status and Potential of Spate Irrigation in Ethiopia,” *Water Resources Management*, vol. 25, no. 7, pp. 1899–1913, May 2011, doi: 10.1007/s11269-011-9780-7.
- [16] H. Bouimouass, Y. Fakir, S. Tweed, H. Sahraoui, M. Leblanc, and A. Chehbouni, “Traditional irrigation practices sustain groundwater quality in a semiarid piedmont,” *Catena (Amst)*, vol. 210, p. 105923, Mar. 2022, doi: 10.1016/j.catena.2021.105923.
- [17] L. S. Pereira, I. Cordery, and I. Iacovides, “Improved indicators of water use performance and productivity for sustainable water conservation and saving,” *Agric Water Manag*, vol. 108, pp. 39–51, May 2012, doi: 10.1016/j.agwat.2011.08.022.
- [18] “Regione Piemonte Cartographic Sector”.
- [19] J. R. Jensen, *Remote Sensing of the Environment: An Earth Resource Perspective 2/e*. Pearson Education, 2009. [Online]. Available: https://books.google.it/books?id=ge_nwDX-HBEC
- [20] M. Shinozuka and B. Mansouri, “Synthetic aperture radar and remote sensing technologies for structural health monitoring of civil infrastructure systems,” in *Structural Health Monitoring of Civil Infrastructure Systems*, Elsevier, 2009, pp. 113–151. doi: 10.1533/9781845696825.1.114.
- [21] G. M. Foody, “Status of land cover classification accuracy assessment,” *Remote Sens Environ*, vol. 80, no. 1, pp. 185–201, Apr. 2002, doi: 10.1016/S0034-4257(01)00295-4.
- [22] P. O. Gislason, J. A. Benediktsson, and J. R. Sveinsson, “Random Forests for land cover classification,” *Pattern Recognit Lett*, vol. 27, no. 4, pp. 294–300, Mar. 2006, doi: 10.1016/j.patrec.2005.08.011.

- [23] M. Pal and P. M. Mather, "Support vector machines for classification in remote sensing," *Int J Remote Sens*, vol. 26, no. 5, pp. 1007–1011, Mar. 2005, doi: 10.1080/01431160512331314083.
- [24] M. Hibjur Rahaman, Roshani, M. Masroor, and H. Sajjad, "Integrating remote sensing derived indices and machine learning algorithms for precise extraction of small surface water bodies in the lower Thoubal river watershed, India," *J Clean Prod*, vol. 422, p. 138563, Oct. 2023, doi: 10.1016/j.jclepro.2023.138563.
- [25] B. Wu, J. Zhang, and Y. Zhao, "A Novel Method to Extract Narrow Water Using a Top-Hat White Transform Enhancement Technique," *Journal of the Indian Society of Remote Sensing*, vol. 47, no. 3, pp. 391–400, Mar. 2019, doi: 10.1007/s12524-018-0910-z.
- [26] "<https://pro.arcgis.com/en/pro-app/latest/tool-reference/spatial-analyst/train-k-nearest-neighbor-classifier.htm>."
- [27] M. Pal, "Random forest classifier for remote sensing classification," *Int J Remote Sens*, vol. 26, no. 1, pp. 217–222, Jan. 2005, doi: 10.1080/01431160412331269698.
- [28] "<https://pro.arcgis.com/en/pro-app/latest/tool-reference/spatial-analyst/train-support-vector-machine-classifier.htm>."
- [29] K. Arai, "Maximum Likelihood Classification based on Classified Result of Boundary Mixed Pixels for High Spatial Resolution of Satellite Images," *International Journal of Advanced Computer Science and Applications*, vol. 11, no. 9, 2020, doi: 10.14569/IJACSA.2020.0110904.
- [30] "<https://pro.arcgis.com/en/pro-app/latest/help/analysis/geoprocessing/modelbuilder/what-is-modelbuilder-.htm>."

